

# 1 How accurately do we know the temperature of the surface 2 of the earth?

3 S. Lovejoy<sup>1</sup> 

4 Received: 31 August 2016 / Accepted: 30 January 2017  
5 © Springer-Verlag Berlin Heidelberg 2017

6 **Abstract** The earth's surface temperature is important in  
7 a variety of applications including for quantifying global  
8 warming. We analyze 6 monthly series of atmospheric tem-  
9 peratures from 1880 to 2012, each produced with different  
10 methodologies. We first estimate the relative error by sys-  
11 tematically determining how close the different series are  
12 to each other, the error at a given time scale is quantified  
13 by the root mean square fluctuations in the pairwise differ-  
14 ences between the series as well as between the individual  
15 series and the average of all the available series. By exam-  
16 ining the differences systematically from months to over a  
17 century, we find that the standard short range correlation  
18 assumption is untenable, that the differences in the series  
19 have long range statistical dependencies and that the error  
20 is roughly constant between 1 month and one century—  
21 over most of the scale range, varying between  $\pm 0.03$  and  
22  $\pm 0.05$  K. The second part estimates the absolute measure-  
23 ment errors. First we make a stochastic model of both the  
24 true earth temperature and then of the measurement errors.  
25 The former involves a scaling (fractional Gaussian noise)  
26 natural variability term as well as a linear (anthropogenic)  
27 trend. The measurement error model involves three terms:  
28 a classical short range error, a term due to missing data  
29 and a scale reduction term due to insufficient space–time  
30 averaging. We find that at 1 month, the classical error is  
31  $\approx \pm 0.01$  K, it decreases rapidly at longer times and it is  
32 dominated by the others. Up to 10–20 years, the missing  
33 data error gives the dominate contribution to the error:  
34  $15 \pm 10\%$  of the temperature variance; at scales  $> 10$  years,

the scale reduction factor dominates, it increases the ampli-  
tude of the temperature anomalies by  $11 \pm 8\%$  (these uncer-  
tainties quantify the series to series variations). Finally,  
both the model itself as well as the statistical sampling and  
analysis techniques are verified on stochastic simulations  
that show that the model well reproduces the individual  
series fluctuation statistics as well as the series to series  
fluctuation statistics. The stochastic model allows us to  
conclude that with 90% certainty, the absolute monthly and  
globally averaged temperature will lie in the range  $-0.109$   
to  $0.127$  °C of the measured temperature. Similarly, with  
90% certainty, for a given series, the temperature change  
since 1880 is correctly estimated to within  $\pm 0.108$  of its  
value.

**Keywords** Global temperature · Uncertainty · Scaling ·  
Stochastic modelling

## 1 Introduction

The atmosphere is a turbulent fluid and the tempera-  
ture and other state variables fluctuate from the age of  
the earth down to milliseconds, in space from the size of  
the planet down to millimeters (see Lovejoy (2015) for a  
review). Global scale temperature estimates rely on sparse  
(i.e. fractal), in situ measurement networks (Lovejoy et al.  
1986; Nicolis 1993; Mazzarella and Tranfaglia 2000) and  
mapping them onto regular grids (e.g. with interpolation  
or Kriging) involves nontrivial space–time homogeneity,  
smoothness and other assumptions. In the satellite era and  
with other suppositions, remotely sensed data may also be  
used (e.g. Mears et al. 2011).

Even the problem of mapping a single spatially point-  
like in situ measurement onto a finite resolution grid is

A1 ✉ S. Lovejoy  
A2 lovejoy@physics.mcgill.ca

A3 <sup>1</sup> Department of Physics, McGill University, 3600 University  
A4 st., Montreal, Que H3A 2T8, Canada 

66 nontrivial. At first sight it would appear that the problem is  
 67 even ill-posed because it seems to be an attempt to change  
 68 the resolution of the data by an infinite factor: from zero  
 69 to tens or hundreds of kilometers. However, such spatially  
 70 point-like data are never point-like in space–time and it is  
 71 the effective space–time resolution that is important. For  
 72 example in the weather regime (i.e. for time scales up to  
 73 the lifetime of planetary structures, typically  $\approx 10$  days),  
 74 the space–time relation is linear or  $2/3$  power law for  
 75 Eulerian and Lagrangian frames respectively (see Love-  
 76 joy and Schertzer 2010, 2013) for both short and extended  
 77 reviews). However for time scales with resolutions longer  
 78 than typical (5–10 day) planetary lifetimes (the mac-  
 79 roweather regime) to a good approximation the space–time  
 80 statistics factorize (Sect. 2.4) so that there is quite differ-  
 81 ent time-scale to space-scale relation (Lovejoy and de Lima  
 82 2015; Lovejoy et al. 2017). The observed spatial scaling  
 83 relations (which are also respected by the GCM models—  
 84 although with slightly different exponents), indicate that  
 85 the regularity and smoothness assumptions made by classi-  
 86 cal geostatistical techniques such as Kriging are not appli-  
 87 cable. Below, we show that a consequence of the scaling is  
 88 the existence of “scale reduction factors” that are nonclassi-  
 89 cal but yet are needed to explain the low frequency part of  
 90 the observations.

91 In addition to problems due to sparse networks and  
 92 unknown or ill-defined space–time resolutions, there are  
 93 also practical issues such as estimating the temperature  
 94 over the ocean and over sea ice and with frequent series  
 95 discontinuities and biases caused by the heat island and  
 96 cool park effects (Parker 2006; Peterson 2003). Sea surface  
 97 temperatures series also have nontrivial issues, see Hausfa-  
 98 ther et al. (2016).

99 Even high quality surface networks such as the US His-  
 100 torical Climatology Network “have an average of six dis-  
 101 continuities per century and not a single station is homo-  
 102 geneous for its full period of record” (Peterson 2003).  
 103 Another potential source of bias is the fact that starting at  
 104 around 1950, the rate of increase of nocturnal (minimum)  
 105 temperature values on land was almost twice as high when  
 106 compared to that of diurnal (maximum) temperature values,  
 107 favouring an increase of duration of the frost-free period in  
 108 many regions of moderate and high latitudes (Kondratyev  
 109 and Varotsos 1995; Efstathiou and Varotsos 2010). See also  
 110 Pielke et al. (2007) who enumerates many other issues and  
 111 Diamond et al. (2013) who reviews their implications.

112 Yet in spite of these problems and in order to provide a  
 113 reliable indicator of the state of the climate, half a dozen  
 114 centennial, global scale surface air temperature estimates  
 115 have been produced. The question of their accuracy is  
 116 essential for many applications, including global warming:  
 117 indeed, one of the oldest climate skeptic arguments against

anthropogenic warming is that the data are unreliable or  
 biased. It is therefore important to quantify their accuracy.

118 We analyse the six best-documented (at the time of anal-  
 119 ysis; May 2015) global, monthly averaged time series. Each  
 120 series was constructed with somewhat different data, with  
 121 different homogenization and gridding assumptions. Since  
 122 no absolute ground truth is available, their authors used  
 123 specific theoretical space–time assumptions and models  
 124 to quantify the accuracy of each temperature series statis-  
 125 tics in order to obtain monthly resolution uncertainty esti-  
 126 mates. Yet historically, when confronted with the measure-  
 127 ment of a new physical quantity—here the global average  
 128 surface temperature—the greatest confidence comes from  
 129 the agreement between qualitatively different and physical  
 130 consistent approaches. We therefore systematically com-  
 131 pare each series with the others determining the relative  
 132 accuracy as functions of scale [Sect. 2; this idea and an  
 133 early spectral result were given in Lovejoy et al. (2013a)].  
 134 This analysis motivates the development of a model for the  
 135 absolute accuracy that is developed in Sect. 3. Whereas in  
 136 Sect. 2, we ask the relative accuracy question: “how well  
 137 do different methods using different empirical inputs agree  
 138 with each other as functions of their time scale?”, in Sect. 3  
 139 we move from relative to absolute estimates of error and  
 140 bias attempting to answer the question “how accurate are  
 141 the data as functions of their time scale?”

142 The explicit treatment of scale is important because  
 143 over the range of between about 10 days and 10 years (the  
 144 macroweather regime) the fluctuations (precisely defined  
 145 below) tend to cancel each other out: increasing fluctua-  
 146 tions tend to be followed by decreasing ones so that tem-  
 147 poral averages (of essentially all atmospheric quantities)  
 148 systematically decrease with scale (Lovejoy 2013; Fig. 2  
 149 below). At scales beyond  $\approx 10$ –20 years (the climate  
 150 regime) the temperature is dominated by anthropogenic  
 151 effects and the fluctuations increase with scale. In addition,  
 152 we conventionally expect that lowering the temporal reso-  
 153 lution by averaging over longer and longer time intervals  
 154 will lead to the convergence of each globally averaged tem-  
 155 perature series to the actual temperature so that with suf-  
 156 ficient averaging (i.e. with low enough temporal resolution)  
 157 and in accord with the central limit theorem, the different  
 158 series are expected to mutually converge. The direct way  
 159 to analyze this is by considering the fluctuations in the dif-  
 160 ferences between the different series and to quantify how  
 161 rapidly they diminish with temporal resolution. The only  
 162 technical complication is that we must use an appropri-  
 163 ate definition of fluctuation. This is because on average,  
 164 the classical fluctuations (defined as differences) can-  
 165 not decrease with scale, so that for our purposes, they are  
 166 inadequate. Instead, we use the somewhat different Haar  
 167 fluctuations.

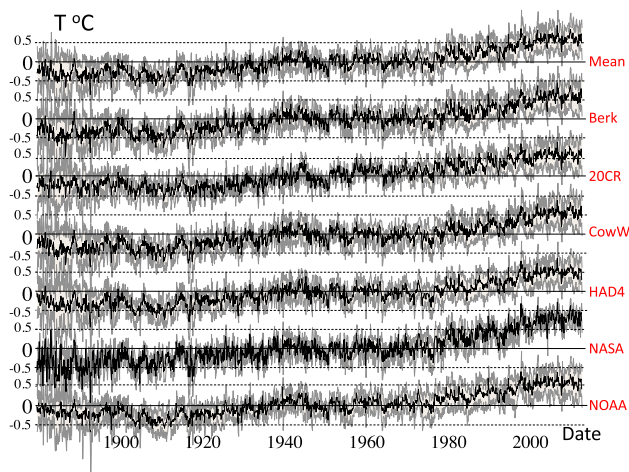


**Fig. 1** The six monthly global surface temperature anomaly series from 1880 to 2012 (*black*) with 3 standard deviation uncertainties in grey with the mean of all six (*top*). From bottom to top: NOAA NCDC, NASA GISS, Hadercrutem4, Cowtan and Way, the 20 Century Reanalysis, the Berkeley series and the overall mean. Each series represents the anomaly with respect to the mean of the entire period, indicated by the *black horizontal axes*. For each of the bottom six series, the uncertainties are determined from the standard deviations of the other five

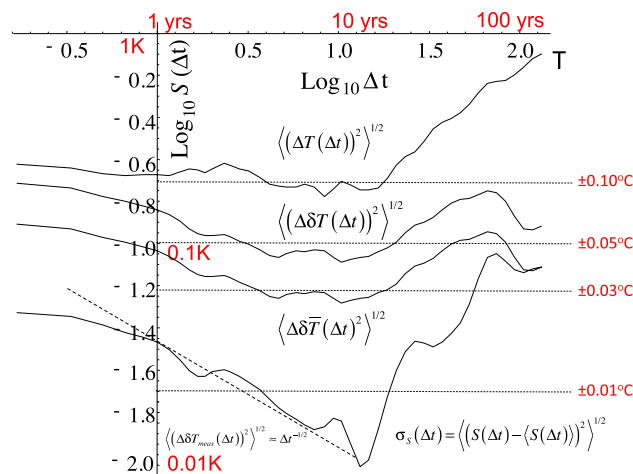


**Fig. 2** The RMS Haar fluctuations  $S(\Delta t)$  averaged over the six series (*top*), averaged over all the 15 pairs of differences (second from *top*), averaged over the differences of each with respect with the overall mean of the six series (third from *top*), and the standard deviation of the  $S(\Delta t)$  curves evaluated for each of the series separately (*bottom*). Also shown for reference (*dashed*) is the line that data with independent Gaussian noise would follow

170 **2 Fluctuation analysis**

171 **2.1 The data**

172 The series that we chose were all publically available at  
 173 monthly resolutions between January 1880 and December  
 174 2012 (133 years=1596 months). They were (a) the  
 175 NOAA NCDC series GHCN-M version 3.2.0 dataset  
 176 (Smith et al. 2008), updated in Williams et al. (2012),  
 177 abbreviated NOAA in the following, (b) the NASA God-  
 178 dard Institute for Space Studies Surface Temperature  
 179 Analysis (GISTEMP) series, abbreviated NASA (Hansen  
 180 et al. 2010), (c) the Combined land and sea surface tem-  
 181 perature (SST) anomalies from HadSST3, Hadley Centre-  
 182 Climatic Research Unit Version 4, abbreviated HAD4  
 183 (Brohan et al. 2006; Kennedy et al. 2011), (d) the version 2  
 184 series of (Cowtan and Way 2014) (abbreviated CowW), (e)  
 185 the Twentieth Century reanalysis, version 2 (Compo et al.  
 186 2011), (20CR) and (f) the Berkeley Earth series (Rohde  
 187 et al. 2013) abbreviated Berk. Shortly after these series  
 188 were analyzed, some of the series were updated (notably by  
 189 Karl et al. 2015), but we are not trying to establish which  
 190 series is best, but rather how the errors vary with scale so  
 191 that the updates are unlikely to alter the conclusions.

192 Each data set has its particular strengths and weak-  
 193 nesses, we enumerate a few of these in order to under-  
 194 line their diversity. For example, NOAA and NASA use  
 195 essentially the same land and marine data, but use differ-  
 196 ent methods to fill (some) of the data holes. In contrast the

HAD4 series makes no attempt in this direction, thus mak- 197  
 ing fewer assumptions about the spatial statistical proper- 198  
 ties (especially smoothness, regularity properties). The 199  
 CowW series takes the contrary view: it uses the HAD4 200  
 data but makes strong spatial statistical assumptions (Krig- 201  
 ing) to fill in data holes. This is especially significant in 202  
 the data poor high latitude regions. The 20CR series is of 203  
 particular interest here because it uses no temperature sta- 204  
 tion data whatsoever. Instead, it uses surface pressure sta- 205  
 tion data and monthly SST data (the same as HADCRUT4) 206  
 combined with a numerical model (a reanalysis), it is the 207  
 only series that gives actual temperatures rather than 208  
 changes with respect to a reference period: “anomalies”. 209  
 The fact that the 20CR agrees well with the other (station 210  
 based temperature) estimates is strong support for all the 211  
 series (Compo et al. 2013). Finally, the Berk series uses 212  
 the same SST data as both HAD4 and CowW but it uses data 213  
 from many more stations ( $\approx 37,000$  compared to only 4500 214  
 for HAD4 and 7300 for the NOAA series for example), and 215  
 it uses a number of statistical improvements in the handling 216  
 of data homogenization and coverage. Our objective here 217  
 is not to attempt to evaluate which assumptions, or which 218  
 products are better—or worse—our point is that there is a 219  
 significant diversity so that the degree of agreement or dis- 220  
 agreement between the various series is of itself important. 221

Figure 1 shows a visual comparison of the series. 222  
 In addition to the temperature (black), we have shown 223  
 uncertainty limits (grey). These are not theoretical esti- 224  
 mates of intrinsic uncertainty but rather the dispersion 225  
 of the five temperature records about the given series 226

(three standard deviations): it measures the series similitude/dissimilitude. Where gray regions extend far above and below the black lines, they indicate that there is little agreement between the curve in question (black) and the other series. Where the band is narrow, it indicates strong agreement. Overall we see that each series is very similar to the others (including the particularly significant 20CR series); comparing any individual curve with that of the overall mean of the six (top curve), we see that no particular series stands out. In addition, before 1900—but also after 1980—the series are the most dissimilar so presumably the least reliable. While this is not surprising for the earlier (data poor) epoch, a priori, it is not obvious in the more recent period. In Sect. 3, it is explained by the differing scale reduction factors.

## 2.2 Anomalies, differences, Haar fluctuations

The uncertainties in Fig. 1 are limited to quantifying the similarities/differences at unique temporal resolutions: 1 month. Since as we go to lower resolutions measurement errors are increasingly averaged, we expect a progressively stronger agreement at longer times. Standard uncertainty analyses (e.g. Kennedy et al. 2011) assume that there are both long term biases and short term errors and that the latter have short-range (exponential) decorrelations (e.g. the errors are auto-regressive or kindred processes). But a growing body of work finds monthly resolution atmospheric fields have long range statistical dependencies (wide range temporal and spatial scaling, power laws, Lovejoy and Schertzer 1986; Bunde et al. 2004; Rybski et al. 2006; Mann 2011; Franzke 2012; Rypdal et al. 2013, see Lovejoy and Schertzer 2013 for a review). The issue of short versus long range correlations also has implications for trend uncertainty analysis, see Lovejoy et al. (2016).

To quantify the resolution effect, denote the true global temperature anomaly by  $T(t)$  (i.e. the actual averaged temperature of the entire planet with the annual cycle removed and the overall mean of the series removed so that  $\langle T \rangle = 0$  where “ $\langle \cdot \rangle$ ” indicates averaging). Define the  $\Delta t$  resolution anomaly fluctuation by:

$$(\Delta T(\Delta t))_{anom} = \frac{1}{\Delta t} \int_{t-\Delta t}^t T(t') dt' \quad (1)$$

have suppressed the  $t$  dependence since we will assume that the fluctuation statistics are statistically stationary; this may be true even though—due to anthropogenic warming—the statistics of the temperature itself are nonstationary. Note that if we have anomaly data at “resolution  $t'$ ”, i.e. averaged over time  $t$ ,  $T_\tau(t)$ , then  $T_\tau = (\Delta T(\tau))_{anom}$  a fact that will use below.

Let us denote the overall deviations from the true value  $E_i(t)$  (we use the term “deviation” to include both biases and errors). Now denote the  $i$ th measured anomaly by:

$$T_i(t) = T(t) + E_i(t) \quad (2)$$

For large enough averaging interval ( $\Delta t$ ), we expect that the deviation  $E$  will be increasingly averaged out so that for the  $i$ th and  $j$ th series  $(\Delta T_i(\Delta t))_{anom} \approx (\Delta T(\Delta t))_{anom} \approx (\Delta T_j(\Delta t))_{anom}$ . Alternatively, by defining the difference:

$$\delta T_{ij}(t) = T_i(t) - T_j(t) = \delta E_{ij}(t) \quad (3)$$

have the simple result  $\delta T_{ij}(t) = E_i(t) - E_j(t)$ . If the deviations  $E_i(t)$ ,  $E_j(t)$  are short range processes (i.e. dominated by standard measurement errors with having exponential decorrelations such as autoregressive processes and their kin), we can use the central limit theorem to conclude that at large enough  $\Delta t$  (where  $E_i(t)$ ,  $E_j(t)$  are statistically independent) that the rate at which the root mean square (RMS) anomaly fluctuation approaches zero is:

$$\langle \Delta \delta T_{ij}(\Delta t)^2 \rangle^{1/2} = \langle \Delta \delta E_{ij}(\Delta t)^2 \rangle^{1/2} \propto \Delta t^{-1/2} \quad (4)$$

If the separation of the deviations into short term errors and long term biases is at all possible, then for large enough averaging scale ( $\Delta t$ ) it should display a  $\Delta t^{-1/2}$  regime for the anomaly fluctuations.

Before testing this prediction on the data, we must first discuss different definitions of fluctuations and their limitations. Anomaly fluctuations must on average decrease with averaging scale  $\Delta t$ , so that are only adequate when the fluctuations decrease with scale  $\Delta t$ . For fluctuations that increase with  $\Delta t$ , we can use the classical definition of fluctuation, the differences:

$$(\Delta T(\Delta t))_{diff} = T(t) - T(t - \Delta t) \quad (5)$$

In contrast to anomaly fluctuations, average differences cannot decrease with scale whereas in general, average fluctuations may either increase or decrease as over different ranges of  $\Delta t$ . We must therefore define fluctuations in a more general way; wavelets provide a fairly general framework for this. A simple expedient combines averaging and differencing while overcoming many of the limitations of each: the Haar fluctuation (from the Haar wavelet). It is simply the difference of the mean over the first and second halves of an interval:

$$(\Delta T(\Delta t))_{Haar} = \frac{2}{\Delta t} \int_{t-\Delta t/2}^t T(t') dt' - \frac{2}{\Delta t} \int_{t-\Delta t}^{t-\Delta t/2} T(t') dt' \quad (6)$$

(see Lovejoy and Schertzer 2012b for these fluctuations in a wavelet formalism). In words, the Haar fluctuation is the

319 difference fluctuation of the anomaly fluctuation, it is also  
 320 equal to the anomaly fluctuation of the difference fluctua-  
 321 tion. In regions where the fluctuations decrease with scale  
 322 we have:

$$\begin{aligned}
 (\Delta T(\Delta t))_{Haar} &\propto T(\Delta t)_{anom} \quad (\text{decreasing with } \Delta t) \\
 (\Delta T(\Delta t))_{Haar} &\propto T(\Delta t)_{diff} \quad (\text{increasing with } \Delta t)
 \end{aligned}
 \tag{7}$$

324 In order that Eq. 7 is reasonably accurate, the Haar fluctua-  
 325 tions need to be multiplied by a “calibration” factor;  
 326 here we use the “canonical” value 2 although a more opti-  
 327 mal value could be tailored to individual series.

328 Over ranges where the dynamics have no characteristic  
 329 time scale, the statistics of the fluctuations are power laws  
 330 so that:

$$\langle |\Delta T(\Delta t)|^q \rangle \propto \Delta t^{\xi(q)} \tag{8}$$

332 The left hand side is the  $q$ th order structure function and  
 333  $\xi(q)$  is the structure function exponent. “ $\langle \rangle$ ” indicates  
 334 ensemble averaging; for individual series this is estimated  
 335 by temporal averaging (over the disjoint fluctuations in the  
 336 series). The first order ( $q = 1$ ) case defines the “fluctuation  
 337 exponent”  $H$ :

$$\langle |\Delta T(\Delta t)| \rangle \propto \Delta t^H \tag{9}$$

339 In the special case where the fluctuations are quasi-  
 340 Gaussian,  $\xi(q) = qH$  and the Gaussian white noise case  
 341 corresponds to  $H = -1/2$  (i.e.  $\xi(q) = -q/2$ ). More gen-  
 342 erally, there will be “intermittency corrections” so that  
 343  $qH - \xi(q) = K(q)$  where  $K(q)$  is a convex function with  
 344  $K(1) = 0$ .  $K(q)$  characterizes the multifractality associated  
 345 with the intermittency.

346 Equation 9 shows that the distinction between increasing  
 347 and decreasing fluctuations corresponds to the sign of  $H$ . It  
 348 turns out that the anomaly fluctuations are adequate when  
 349  $-1 < H < 0$  whereas the difference fluctuations are adequate  
 350 when  $0 < H < 1$  (Lovejoy and Schertzer 2013, ch. 5). In  
 351 contrast, the Haar fluctuations are useful over the range  
 352  $-1 < H < 1$  which encompasses virtually all geoprocesses,  
 353 hence its more general utility. When  $H$  is outside the indi-  
 354 cated ranges, then the corresponding statistical behaviour  
 355 depends spuriously on either the extreme low or extreme  
 356 high frequency limits of the data.

### 357 2.3 Temporal analysis and the relative measurement 358 errors

359 Figure 2 (top curve), shows the result when we estimate the  
 360 Haar temperature fluctuations and average them over all the  
 361 available disjoint intervals  $\Delta t$  and over all the series, calcu-  
 362 lating the RMS Haar fluctuation:

$$S(\Delta t) = \langle (\Delta T(\Delta t))_{Haar}^2 \rangle^{1/2} \tag{10}$$

the “structure function”: below we drop the subscripts,  
 all fluctuations are Haar. In a scaling regime, we there-  
 fore have:

$$S(\Delta t) \propto \Delta t^{\xi(2)/2} \tag{11}$$

If the intermittency is small ( $K(q) \approx 0$ ), then  $\xi(2)/2 \approx H$   
 and  $S(\Delta t) \propto \Delta t^H$ . Note that we estimate  $S(\Delta t)$  using all  
 available disjoint intervals of size  $\Delta t$ . Since the number  
 of disjoint intervals decreases as  $\Delta t$  increases, so does the  
 sample size, hence the statistics are less reliable at large  
 $\Delta t$  explaining the somewhat “noisy” appearance of plots  
 such as Fig. 2 or 3. The only way to completely quantify  
 this effect is with a stochastic model of the process; this  
 is done in Sect. 3.

Starting at the smallest (monthly) scales with fluctua-  
 tions  $\approx \pm 0.14$  K, the latter decrease slowly to  $\approx 10$   
 years, (roughly as  $\Delta t^H$ , with  $H \approx -0.1$  see Lovejoy and  
 Schertzer (2012a) and below) whereas for  $\Delta t > \approx 10$  years  
 they increase. This increase reflects the increasing domi-  
 nance of anthropogenic forcing over the natural variabil-  
 ity (Lovejoy et al. 2013b). How accurate is this curve?  
 Figure 3 (top set) shows the individual  $S(\Delta t)$  functions  
 for each of the series, we see that they are very close.  
 The bottom curve in Fig. 2 quantifies this closeness  
 by determining the standard deviation  $\sigma_S$  of the  $S(\Delta t)$   
 curves about the ensemble mean at the top of Fig. 2.  
 We see that—as expected— $\sigma_S$  decreases as  $\Delta t^{-1/2}$ —  
 but only over the range over which natural variability is  
 dominant—becoming as low as  $0.01$  °C ( $\pm 0.005$  °C) at  
 decadal scales. At the longer time scales, the standard  
 deviation increases implying a disagreement over the  
 magnitude of multi-decadal and centennial variability

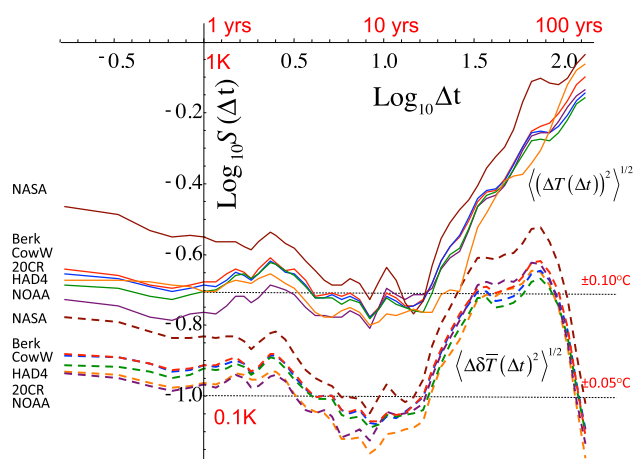


**Fig. 3** The top set of curves (solid) are  $S(\Delta t)$  for each of the differ-  
 ent series, the bottom set (dashed) are the differences of each with  
 respect to the mean of all the others: NOAA dark purple, NASA  
 (brown), HAD4 (green), Cow (blue), 20CR (orange), Berk (red)  
 (indicated at the left in the order of the curves)

395 i.e. disagreements of the order 0.06 to 0.1 K ( $\pm 0.03$  to  
396  $\pm 0.05$  K) for the total anthropogenic forcing.

397 In most applications, we are interested in the accuracy of  
398 the *temperature anomalies* themselves whereas the bot-  
399 tom curve in Fig. 2 only tells us about the accuracy of our  
400 estimate of their RMS *statistics*. To characterize the for-  
401 mer, we analyze the fluctuations of the differences between  
402 series:  $\Delta\delta T_{ij}(\Delta t)$  (Eq. 3) or alternatively, between the  $i$ th  
403 series and the mean  $\langle T(t) \rangle$  of all the series:

$$404 \delta\bar{T}_i(t) = T_i(t) - \langle T(t) \rangle \quad (12)$$

405 The second curve from the bottom is the RMS of the lat-  
406 ter over all the series is:  $\langle \Delta\delta\bar{T}(\Delta t)^2 \rangle^{1/2}$ . In Fig. 2, the third  
407 curve from the bottom is the RMS of  $\Delta\delta T_{ij}(\Delta t)$  averaged  
408 over all the pairs of series:  $\langle (\Delta\delta T(\Delta t))^2 \rangle^{1/2}$  (for  $N$  series,  
409 there are  $N(N-1)/2$  pairs, here  $N=6$  so that there are 15  
410 pairs). Whereas  $\langle (\Delta\delta T(\Delta t))^2 \rangle^{1/2}$  quantifies the typical dif-  
411 ference between any two randomly chosen series at resolu-  
412 tion  $\Delta t$ ,  $\langle \Delta\delta\bar{T}(\Delta t)^2 \rangle^{1/2}$  is the typical  $\Delta t$  resolution devia-  
413 tion of a series when the mean of all the series is considered  
414 the truth. A similar approach was recently used to estimate  
415 relative errors in climatological precipitation series in (de  
416 Lima and Lovejoy 2015).

417 Figure 2 shows a rather surprising result. While at first  
418 (from months to about 3–4 years), as expected—at least  
419 initially—the series do converge (they become closer to the  
420 overall mean), they do so considerably more slowly than  
421 expected for series with short range correlations. Rather  
422 than converging as  $\Delta t^{-1/2}$  (Eq. 4), they converge as  $\approx \Delta t^{-0.2}$   
423 indicating long range statistical dependencies, confirm-  
424 ing earlier results obtained using spectra (Lovejoy and  
425 Schertzer 2013) (appendix 10 C; scaling fluctuations imply  
426 power law spectra  $E(\omega) \approx \omega^{-\beta}$  with  $\beta = 1 + \xi(2)$  where  $\omega$   
427 is the frequency). Ignoring small intermittency correc-  
428 tions,  $\beta = 1 + 2H$  so that a “flat”  $S(\Delta t)$  curve ( $\xi(2) \approx 0$ )  
429 indicates a spectrum  $E(\omega) \approx \omega^{-1}$ . However, in the scale  
430 range  $\Delta t \approx 10$ – $20$  years dominated by anthropogenic  
431 effects, the differences begin to *increase* and over the entire  
432 range of time scales, there is an irreducible (minimum)  
433 error  $\approx \pm 0.03^\circ\text{C}$  to  $\pm 0.05^\circ\text{C}$ . Since the standard theory  
434 predicts a  $\Delta t^{-1/2}$  fall-off: it fails at all scales so that different  
435 sources of error must be dominant (the effect of the finite  
436 sample size that decreases at larger  $\Delta t$  slightly increases  
437 the “noisiness” of the curves at larger  $\Delta t$ , and is probably  
438 responsible for the small downturn in the  $S(\Delta t)$  curves of  
439 the differences at  $\Delta t \approx > 100$  years). Indeed, the standard  
440 theory predicts centennial scale deviations of  $\approx \pm 0.002^\circ\text{C}$   
441 rather than the observed  $\pm 0.03^\circ\text{C}$  to  $\pm 0.05^\circ\text{C}$  (third curve,  
442 from the top, extreme right). Figure 2 also brings into ques-  
443 tion the utility of attempting to break the deviation into dis-  
444 tinct short term measurement error and long term measure-  
445 ment bias components. The combination of error and bias  
446 is apparently present at all scales.

447 Figure 2 shows how any series differs from any other as  
448 well from the best estimate of the truth: the average over all  
449 of them. However, we may further quantify the monthly  
450 spreads in Fig. 1: for any given series, how close is it to the  
451 mean of the others (the relative measurement errors)?  
452 Fig. 3 shows the result: the top gives  $\langle \Delta T_i(\Delta t)^2 \rangle^{1/2}$  for  
453 each of the six curves; we see that these statistics are indeed  
454 very similar (their dispersion is quantified in the bottom  
455 curve of Fig. 2). Note that the NASA curve has the steepest  
456 slope in the macroweather region ( $\Delta t \approx < 10$ – $20$  years) cor-  
457 responding to  $H \approx -0.2$  rather than  $H \approx -0.1$  for the oth-  
458 ers. More interesting is the bottom set of curves  
459  $\langle \delta\bar{T}_i(\Delta t)^2 \rangle^{1/2}$ , the difference between the  $i$ th series and the  
460 mean of the other five. From the top set we see that gener-  
461 ally the NOAA and 20CR series have the weakest variabil-  
462 ity (top curves) whereas the NASA and Berk series have  
463 the strongest. From the bottom set we see that the NOAA  
464 and 20CR series are the closest to the other series whereas  
465 the NASA, Berk and CowW are the furthest (the most dif-  
466 ferent). Aside from its obvious interpretation in terms of  
467 similitude and difference from one series to another, the  
468 statistics of  $\langle \delta\bar{T}_i^2 \rangle^{1/2}$  will later be compared with the same  
469 quantity from stochastic simulations (Sect. 3) in order to  
470 validate them.

#### 471 2.4 Space–time fluctuations, statistical factorization 472 and the scale reduction factor

473 The differences between the series are due to the quan-  
474 tity and quality of the data that they use and the assump-  
475 tions they use in order to grid them and then to space–time  
476 average them. In terms of the statistics of the resulting  
477 series, the former effect is largely associated with differ-  
478 ent amounts of missing data while the latter will affect the  
479 effective space–time resolution of the data. Both of these  
480 effects are important in modelling the errors; to model their  
481 effects, we require knowledge of the space–time statistics.

482 A space–time analysis of the 20th C reanalysis of the  
483 absolute temperatures (with only annual detrending) was  
484 already given in ch. 10 of (Lovejoy and Schertzer 2013).  
485 However, for our present purposes, the statistics of tem-  
486 perature anomalies—not temperature data—is needed;  
487 we therefore used the HADcrut anomaly data from 1880  
488 at  $5^\circ \times 5^\circ$  spatial resolution. Figure 4 shows the result of  
489 estimating the RMS Haar spatial fluctuations over vari-  
490 ous spatial resolutions in the zonal direction, for the latter,  
491 the difference in the longitudinal angle  $\Delta\theta$  was used, the  
492 fluctuation statistics being averaged over all latitudes from  
493  $60^\circ\text{S}$  to  $60^\circ\text{N}$  (weighted by the grid box size—the latitude  
494 dependent map factor).

495 The top (monthly) resolution curve shows that the fluc-  
496 tuations decrease with increasing spatial scale. Since only

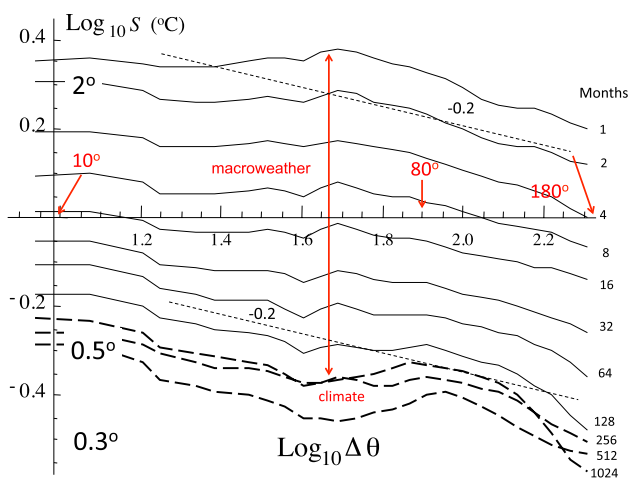


**Fig. 4** The zonal spatial analysis of the HADCrut surface data (on a  $5^\circ \times 5^\circ$  grid) as functions of temporal averaging (systematically doubling from 1 month to 1024 months  $\approx 85$  years, top to bottom). Although it is “noisy”, roughly the effect of temporal averaging is the decrease the amplitude of the fluctuations at all spatial scales. This is as predicted by the macroweather space–time factorization property. The double headed arrow shows the predicted downward shift from 1 to 128 months (red curves) with temporal  $H_t = -0.3$ . The reference line has slope  $\xi_x(2)/2 = -0.2$

497  $\approx 40\%$  of the pixels had data, we used a Haar fluctuation  
 498 algorithm that takes into account the missing data (“Appendix  
 499 A” of Lovejoy 2015). This is important since if the data  
 500 are interpolated, then the result is too smooth and can give  
 501 spurious scaling (a smooth curve will have a Haar exponent  
 502  $H = 1$  rather than  $H < 0$  as in the data).

503 From Fig. 4 we can see that as the spatial resolution  
 504 ( $\Delta\theta$ ) is increased, the anomaly fluctuations decrease  
 505 with scale roughly as:  $S_\theta(\Delta\theta) \propto \Delta\theta^{\xi(2)/2}$  with  $\xi(2) =$   
 506  $-0.4$ . To interpret this result, recall that the spatial fluctuation  
 507 exponent  $H_s = \xi(1)$  is defined in terms of the mean (i.e. first order  
 508 moment):  $\langle |\Delta T(\Delta\theta)| \rangle \propto \Delta\theta^{H_s}$ . Whereas in the macroweather  
 509 regime the temporal RMS and mean fluctuation exponents are nearly  
 510 equal ( $\langle \Delta T(\Delta t)^2 \rangle^{1/2} \propto \langle \Delta T(\Delta t) \rangle \propto \Delta t^{H_t}$ ; low  
 511 intermittency,  $K(q) = 0$ ; see the discussion after Eq. 9)—the spatial  
 512 fluctuations are on the contrary highly intermittent (see e.g. section  
 513 10.3.1 of Lovejoy and Schertzer (2013) so that the quasi  
 514 Gaussian approximation no longer holds. In space there is  
 515 an intermittency correction  $\xi(2)/2 - \xi(1) = \xi(2)/2 - H_s \approx$   
 516  $-0.1$  so that  $\langle \Delta T(\Delta\theta)^2 \rangle^{1/2} \propto \langle \Delta T(\Delta\theta) \rangle^{-0.1} \propto \Delta\theta^{H_x - 0.1}$ ,  
 517 the graphical estimate in Fig. 4 ( $\xi(2)/2 \approx -0.2$ ) thus implies  
 518  $H_x \approx -0.1$ . Since  $H_x < 0$ , both the mean—and the RMS  
 519 fluctuations—decrease with scale  $\Delta\theta$ . (the spatial subscript  
 520 “x” is used since we presume that the zonal angular separation  
 521  $\Delta\theta$  is approximately equal to the great circle distance  
 522  $\Delta x$ ).

524 Also shown in Fig. 4 is the effect of increasing the temporal  
 525 averaging, systematically doubling it from 1 month to

1024 months ( $\approx 85$  years). The temporal fluctuations have  
 $H < 0$ , so that the temporal fluctuation is simply the anomaly  
 at that scale (equal to the temporal average) so that Fig. 4  
 effectively represents the joint space–time RMS fluctuations  
 $S_{x,t}(\Delta\theta, \Delta t)$ . In ch. 10 of (Lovejoy and Schertzer 2013;  
 Lovejoy and de Lima 2015) it is argued on both theoretical  
 and empirical grounds (monthly temperatures from the 20CR)  
 that to a good approximation, the space–time statistics  
 factorize. For the second order statistics, this implies:

$$S_{x,t}(\Delta\theta, \Delta t) \propto S_x(\Delta\theta)S_t(\Delta t) \quad (13)$$

Where  $S_x(\Delta\theta)$  and  $S_t(\Delta t)$  are respectively the space only  
 and time only RMS structure functions (we have temporarily  
 added the subscript “t”: elsewhere we continue to denote the  
 time only RMS structure function simply by  $S(\Delta t)$ ). Since  
 $\log S_{x,t}(\Delta\theta, \Delta t) \approx Const. + \log S_x(\Delta\theta) + \log S_t(\Delta t)$ ,  
 plot of  $\log \Delta\theta$  versus  $\log S_{x,t}(\Delta\theta, \Delta t)$ , factorization  
 implies that for various time resolutions  $\Delta t$ , the curves  
 for  $\log S_{x,t}(\Delta\theta, \Delta t)$  are simply displaced downwards by  
 $\log S_t(\Delta t)$ . We can see that this is relatively well confirmed  
 in Fig. 4. In addition, due to the temporal macroweather  
 scaling (Fig. 3 for the global series up to about  $\approx 10$ – $20$   
 years), we expect  $S_t(\Delta t)$  also to be a power law so that the  
 in macroweather regime, the curves will be roughly equally  
 spaced as the averaging time  $\Delta t$  is doubled. From the figure,  
 we find (up to  $\Delta t \approx 256$  months, i.e.  $\approx 20$  years and  
 from  $\approx 20^\circ$  to  $180^\circ$  longitude):

$$S_{\theta,t}(\Delta\theta, \Delta t) \propto \Delta\theta^{H_x} \Delta t^{H_t}; \quad H_x \approx -0.2; \quad H_t \approx -0.3 \quad (14)$$

i.e. we have factorization and space–time scaling. Similar  
 space–time factorization (but with different exponents) was  
 found to hold in historical precipitation data (Lovejoy and  
 de Lima 2015).

In order to understand the physical meaning of space–time  
 factorization, recall that in the weather regime the appropriately  
 nondimensionalized structure function has a form (very roughly):  
 $S_{x,t}(\Delta\theta, \Delta t) \propto (\Delta\theta^2 + \Delta t^2)^{s/2}$  (see Pinel et al. 2014  
 for more precise, general results). This implies that the same  
 amplitude of fluctuation  $S_{x,t}$  will typically result from either  
 an instantaneous spatial displacement  $L$  (i.e. with space–time  
 lag  $(L, 0)$ ), or from a temporal lag  $\tau$  at a fixed location  
 (with space–time lag  $(0, \tau)$ ). Mathematically, it implies that  
 there is a size ( $L$ )–lifetime ( $\tau$ ) relationship which is the  
 solution of implicit equation  $S_{x,t}(L, 0) = S_{x,t}(0, \tau)$ ; in  
 this nondimensionalized example the relation is:  $L = \tau$ . In  
 contrast, in the macroweather regime, due to factorization,  
 the corresponding implicit relation between  $L$  and  $\tau$  is  
 $S_x(L)S_t(0) = S_x(0)S_t(\tau)$  whose solution will depend  
 on the spurious small  $L$  and small  $\tau$  behaviours (where for  
 example, the scaling laws break down). To avoid this technical  
 issue (in this case with both  $H_x$  and  $H_t < 0$ ), instead of  
 structure functions, we can use

577 autocorrelation functions to obtain new (nondimensional)  
578 macroweather space–time relations:  $\tau \propto L^{H_x/H_t}$  (Lovejoy  
579 et al. 2017).

580 Notice that the above temporal exponent ( $H_t = -0.3$ )—  
581 which is the exponent of  $5^\circ \times 5^\circ$  resolution data—is  
582 smaller than the corresponding exponent of the globally  
583 averaged series (in Fig. 2 it is  $H_t \approx -0.1$ , see Sect. 3 for a  
584 more accurate estimate). The reason for this apparent dis-  
585 crepancy is that the temporal exponent  $H_t$ —while remain-  
586 ing in the range  $0 > H_t > -1/2$ —varies considerably from  
587 region to region with the oceans typically having  $H_t \approx -0.1$   
588 whereas land typically has  $H_t \approx -0.3$ . As we increase spa-  
589 tial averaging from  $5^\circ \times 5^\circ$  to global, the higher (ocean)  
590 exponents tend to dominate so that for globally averaged  
591 temperatures  $H_t \approx -0.1$ .

592 The space–time macroweather statistics will be more  
593 fully investigated elsewhere, for this paper, the key point is  
594 that both the spatial and temporal  $H$ 's are negative. When  
595  $H < 0$ , then we saw (Eq. 1) that the temperature at resolu-  
596 tion  $\tau$  will scale with exponent  $H$ , i.e. as  $\tau^H$  ( $H < 0$ ). Hence  
597 if a measured series “ $m$ ” is not sufficiently averaged or on  
598 the contrary, perhaps over-smoothed by interpolation, then  
599 it's effective resolution  $\tau_m$  will be different from the nomi-  
600 nal resolution  $\tau_n$  and  $T_{\tau_m}/T_{\tau_n} \approx \lambda_t^{H_t}$  where  $\lambda_t = \tau_m/\tau_n$  is the  
601 resolution scale ratio. Since the spatial exponent  $H_x < 0$ , the  
602 same argument applies in space (resolutions  $\Theta_m, \Theta_n$ ) so that  
603 overall the statistics of the measured anomalies differ from  
604 the true anomalies by the multiplicative factor:

$$605 \quad T_{\tau_m, \Theta_m}/T_{\tau_n, \Theta_n} \approx \lambda_t^{H_t} \lambda_x^{H_x} = e^{\delta u} \quad (15)$$

606 we have introduced  $\delta u$  which is a convenient characteriza-  
607 tion of the overall space–time factor  $\lambda_t^{H_t} \lambda_x^{H_x}$ . The “ $\delta$ ” is to  
608 remind us that  $\delta u$  is due to a difference in the logarithms  
609 of the scaling factors. When  $\delta u$  is not too far from zero—as  
610 here—we have  $e^{\delta u} \approx 1 + \delta u$ , below we empirically estimate  
611  $\delta u$ . Note that conventional geostatistical methods such as  
612 Kriging assume that at small scales, the fields are smooth—  
613 that there are no resolution dependencies. This implies that  
614  $\delta u = 0$  and as we see below, it explains their inability to  
615 explain the low frequency divergences of the series.

616 In the precipitation literature, this type of resolution  
617 dependent multiplicative factor (when of purely of spatial  
618 origin) is called an “areal reduction factor” (for scaling  
619 approaches to this, see e.g. (Bendjoudi et al. 1997; Venezi-  
620 ano and Langousis 2005). The analysis in Fig. 4 shows that  
621 more generally we may expect analogous “scale reduction”  
622 factors to appear when comparing two different anomaly  
623 temperature series that have different effective space–time  
624 resolutions. Two global time series with different effective  
625 resolutions will have statistics that multiplicatively differ  
626 over their entire range of scales, this scale reduction factor  
627 therefore leads to an overall bias in the statistics.

### 3 The absolute errors 628

#### 3.1 Fractional Gaussian Noise (fGn) 629

630 The previous section compared the relative errors of six  
631 global monthly temperature series. We found that the  
632 dominant statistical behavior of the differences between  
633 the series  $\delta T_{ij}$  cannot be explained by the usual dichot-  
634 omy of (short term) error and (long term) bias. In order to  
635 understand this and to estimate the absolute measurement  
636 errors, we need a model of both the actual temperature  
637 and the measurement process. We have cited now numer-  
638 ous studies that show that the temperature is scaling  
639 over the macroweather regime (Lovejoy and Schertzer  
640 2013), has argued macroweather temporal intermittency  
641 is low and (Lovejoy et al. 2015b) has shown that for  
642 macroweather time series, the simplest scaling model;  
643 fractional Gaussian noise (fGn) is a reasonable approxi-  
644 mation (at least if we ignore the extremes) and that the  
645 long range memory implicit in the scaling can be used for  
646 forecasting purposes. It may be useful to note that fGn is  
647 related by differentiation to the more familiar Fractional  
648 Brownian motion (fBm) process.

649 For our purposes, an fGn process  $G_H(t)$  with parameter  
650  $H$ , is defined as:

$$651 \quad G_H(t) = \frac{c'_H}{\Gamma(1/2+H)} \int_{-\infty}^t (t-t')^{-(1/2-H)} \gamma(t') dt'; \quad -1 < H < 0 \quad (16)$$

652  $\gamma(t)$  is a unit Gaussian “ $\delta$  correlated” white noise with  
653  $\langle \gamma \rangle = 0$  and:

$$654 \quad \langle \gamma(t) \gamma(t') \rangle = \delta(t-t') \quad (17)$$

655 where “ $\delta$ ” is the Dirac function and  $\Gamma$  is the usual gamma  
656 function. The constant  $c'_H$  is a constant chosen so as to  
657 make the expression for the statistics particularly simple.  
658 Details of this and other, useful properties of fGn are briefly  
659 summarized in “Appendix A”. A longer review of the prop-  
660 erties relevant for macroweather modelling and forecasting  
661 are given in (Lovejoy et al. 2015b) and full mathematical  
662 treatment is available in (Biagini et al. 2008). From Eq. 16,  
663 it can be seen that in our range of interest ( $-1/2 < H < 0$ ),  
664  $G_H$  is a smoothed white noise; like the Dirac function and  
665  $\gamma(t)$  it is a generalized function that is strictly only mean-  
666 ingful when integrated over a finite set.

667 The properties of fGn needed below are:

- 668 1.  $G_H(t)$  is statistically stationary.
- 669 2. The mean vanishes:  $\langle G_H^{(s)}(t) \rangle = 0$ .
- 670 3. When  $H = -1/2$ , the process  $G_{-1/2}^{(s)}(t)$  is simply a  
671 Gaussian white noise.



- 672 4. Anomaly fluctuations:  $G_{H,\tau}(t) = \frac{1}{\tau} \int_{t-\tau}^t G_H(t') dt'$  sat-  
 673 isfy:  $\langle G_{H,\tau}(t)^2 \rangle \propto \tau^{2H}$ ;  $-1 < H < 0$ .
- 674 5. It follows that in the small scale limit ( $\tau > 0$ ), the vari-  
 675 ance diverges and  $H$  is scaling exponent of the root  
 676 mean square (RMS) value. This singular small scale  
 677 behaviour is responsible for the strong power law res-  
 678 olution effects in fGn.
- 679 6. Sample functions  $G_{H,\tau}(t)$  fluctuate about zero with  
 680 successive fluctuations tending to cancel each other  
 681 out.
- 682 7. Differences: in the large  $\Delta t$  limit:  $\langle G_{H,\tau}(\Delta t)_{diff}^2 \rangle \propto$   
 683  $2\tau^{2H} \left( 1 - (H+1)(2H+1) \left( \frac{\Delta t}{\tau} \right)^{2H} \right)$ .
- 684 8. Haar fluctuations  $\langle G_{H,\tau}(\Delta t)_{Haar}^2 \rangle = \Delta t^{2H}$ ;  $\Delta t \geq 2\tau$ .  
 685 the normalization  $c'$  (Appendix A"), this result is  
 686 exact.
- 687 9. This implies that Haar fluctuations at time scale  $\Delta t$   
 688 scale as  $\Delta t^{2H}$  and do not depend on the resolution  $\tau$ ,  $H$   
 689 is the fluctuation exponent (Eq. 9).
- 690 10. In usual treatments, of fGn, the parameter  $H$  is the  
 691 fluctuation exponent of the fBm whose increments are  
 692 the corresponding fGn. This conventional fGn param-  
 693 eter  $H$  is thus one larger and is confined to the range  
 694  $0 \leq H \leq 1$ . Here, we define  $H$  more generally as the  
 695 fluctuation exponent (Eq. 9), this allows the definition  
 696 to also be valid for nonGaussian, intermittent multi-  
 697 fractal processes.

### 3.2 Modelling the earth's temperature

701 Having defined the basic statistically stationary scaling  
 702 process (fGn), we need only add a nonstationary process to  
 703 represent the anthropogenic warming. In Lovejoy (2014) it  
 704 was shown that anthropogenic effects were roughly linear  
 705 in the  $\text{CO}_2$  radiative forcing ( $\log \text{CO}_2$ ) rather than linear in  
 706 time. The theoretical justification was that—due to eco-  
 707 nomic activity— $\text{CO}_2$  concentration is a reasonable proxy  
 708 for all the anthropogenic effects. It would thus be better to  
 709 model the anthropogenic part as a contribution linear in  
 710  $\log \text{CO}_2$ —i.e. to replace the time axis by  $\log \text{CO}_2$ . However  
 711 for simplicity, here we will use a term linear in time:

$$T(t) = \sigma_T G_H(t) + At \tag{18}$$

713 where  $t$  is the time in units of months and  $\sigma_T$  is the RMS  
 714 Haar month to month fluctuation,  $G_H$  is an fGn process

and  $A$  is a linear approximation to the anthropogenic trend.  
 With this model, the temperature fluctuates about the mean  
 $\langle T(t) \rangle = At$ . However, as analyzed and underlined in Love-  
 joy et al. (2016), even though on (ensemble) average, fGn  
 is trendless, on each realization, it displays a random trend  
 that will contribute some uncertainty to estimates of global  
 warming.

Using Eqs. 17, 18, the Haar structure function of the  
 model earth temperature yields:

$$S^2(\Delta t) = \langle \Delta T(\Delta t)^2 \rangle = \sigma_T^2 \Delta t^{2H} + A^2 \Delta t^2 \tag{19}$$

(we have used property 8 of Sect. 3.1 and the fact that the  
 Haar fluctuation of the function  $At$  is  $A\Delta t$ ). From the empir-  
 ical structure functions (Figs. 2, 3) if we regress  $S(\Delta t)$   
 between 8 months and 12 years (this avoids the low fre-  
 quency part dominated by the anthropogenic contribution),  
 we get the  $H$  estimate:

$$H = -0.090 \pm 0.042 \tag{20}$$

Taking  $H = -0.1$  and fitting the other parameters, we  
 obtain:

$$A = (5.83 \pm 0.073) \times 10^{-4} \text{ K/month}; \sigma_T = 0.142 \pm 0.01 \text{ K} \tag{21}$$

Where the uncertainty estimates come from the  
 six different series. This value of  $A$  corresponds to  
 $0.700 \pm 0.009$  K/century. With these parameters, in the  
 model (Eq. 18), we made the simulation in Fig. 5.

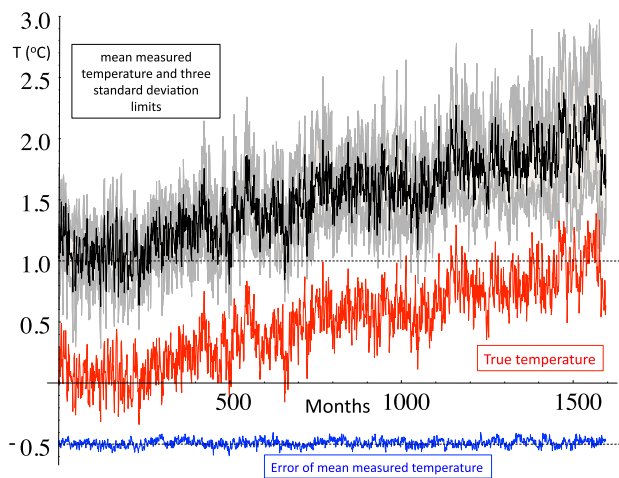


Fig. 5 Red is “true earth” (model) temperature using Eqs. 18 the parameters of Eqs. 20, 21. Black is the mean of six simulations of the measurement process (Sect. 3.4) with 3 standard deviation spreads (gray) and shifted one unit upwards. Blue is the difference between the mean measured temperature and the true temperature (displaced 0.5 downward)

### 739 3.3 Modelling the measurement errors and biases

740 The usual approach to temperature measurement uncertain- 787  
 741 ties is to consider measurement errors that are essentially 788  
 742 white noises i.e.  $G_{-1/2}(t)$ , (i.e.  $H = -1/2$ ). This includes 789  
 743 those with short range (exponential) decorrelations such 790  
 744 as Auto Regressive (AR) processes and their kin. The latter 791  
 745 are essentially white noises for scales larger than their 792  
 746 decorrelation distances/times. In addition, from the dis- 793  
 747 cussion in Sect. 2.4, due to the scale reduction factors, 794  
 748 we expect there to be multiplicative biases  $e^{\delta u}$  effective  
 749 over the entire range of time scales. Since these are close  
 750 to unity,  $e^{\delta u} \approx 1 + \delta u$ . Although  $\delta u$  does depend on how  
 751 missing data is dealt with, it does not exhaust the effects of  
 752 sparse measurements. Recall that over the period 1880-pre-  
 753 sent, at  $5^\circ \times 5^\circ$  resolution there are typically  $>50\%$  missing  
 754 data and different series have different degrees of missing  
 755 data, this is an important additional effect. Since (roughly)  
 756 the space-time statistics factor and are scaling (Sect. 2.4),  
 757 the effect of the missing data is thus to add a third compo-  
 758 nent to the error, one which is expected to be of the same  
 759 statistical type as the natural variability i.e. to be propor-  
 760 tional to an fGn process. These considerations suggest the  
 761 following measurement model:

$$762 T_i(t) = T(t)(1 + \delta u_i) + \sigma_T B_i G_H^{(i)}(t) + \sigma_T \varepsilon_i G_{-1/2}^{(i)}(t) \quad (22)$$

763 Where  $T_i$  is measured temperature from the  $i$ th global 800  
 764 temperature series (here  $i = 1, 6$  for the six series discussed 801  
 765 in Sect. 2) and  $T(t)$  is true global temperature (Eq. 18). 802  
 766 The first term on the right is the scale reduction factor, the 803  
 767 second term is the missing data term and the third is the 804  
 768 short range measurement error term. The latter terms have 805  
 769 been nondimensionalized using the typical monthly (Haar) 806  
 770 variance  $\sigma_T$  (Eq. 18) and the nondimensional amplitudes of  
 771 these noises are denoted  $B_i, \varepsilon_i$  respectively.

772 Taking  $T(t)$  as the earth model (Eq. 18), we obtain:

$$773 T_i(t) = \sigma_T (1 + \delta u_i) G_H^{(0)}(t) + A(1 + \delta u_i)t + \sigma_T B_i G_H^{(i)}(t) + \sigma_T \varepsilon_i G_{-1/2}^{(i)}(t) \quad (23)$$

774 The  $G_H^{(0)}$  is the realization of the fGn that determined 811  
 775 the true temperature of the earth (Eq. 18); in the following 812  
 776 we use the empirical estimate (Eq. 20)  $H = -0.1$  through- 813  
 777 out. Since  $\langle G_H \rangle = 0$ ,  $T_i(t)$  fluctuates around a line with 814  
 778 slope  $A(1 + \delta u_i)$ . 815

779 In order to statistically test the full model (i.e. the model 816  
 780 of the earth temperature plus measurement errors; Eqs. 22, 817  
 781 23) we only need the statistical distribution of the param- 818  
 782 eters  $\delta u_i, B_i, \varepsilon_i$ . For this, we will make some simplifying 819  
 783 assumptions: (a) that each has a Gaussian distribution, 820  
 784 mean  $\mu$ , standard deviation  $\sigma$ , (b) that for each individual 821  
 785 series, the parameters  $\delta u_i, B_i, \varepsilon_i$  are statistically independ-  
 786 ent of each other. In the development below, there is a

further independence assumption, that for pairs of different 787  
 series  $i, j$ , these terms are statistically independent of each 788  
 other. Since the series share much data, this last assumption 789  
 is clearly not fully justified. However, this really affects our 790  
 interpretation of the results, we are in fact making a statisti- 791  
 cal estimate of the *effective* parameters, i.e. the parameters 792  
 that *would* be needed in order to explain the observations *if* 793  
*the series were indeed independent*. 794

### 795 3.4 Estimating the measurement errors and biases

796 A simple way to estimate the measurement model paramete-  
 797 rs  $\delta u_i, B_i, \varepsilon_i$  is to consider the temporal (Haar) fluctuation  
 798 for each series:

$$799 \Delta T_i(t) = \sigma_T (1 + \delta u_i) \Delta G_H^{(0)}(\Delta t) + A(1 + \delta u_i) \Delta t \quad (24)$$

$$+ \sigma_T B_i \Delta G_H^{(i)}(\Delta t) + \sigma_T \varepsilon_i \Delta G_{-1/2}^{(i)}(\Delta t)$$

800 In the following, we attempt to estimate the statistics of  
 801  $\delta u_i, B_i, \varepsilon_i$  from structure functions estimated from the time  
 802 intervals from single series rather than ensemble (statisti-  
 803 cal) averaging. To make this distinction clear for time aver-  
 804 aging we use the overbar “ $\overline{\quad}$ ”. For example, the time aver-  
 805 aged (squared) fluctuation (structure functions) are thus:

$$806 S_i^2(\Delta t) \approx \overline{\Delta T_i(\Delta t)^2} = S^2(\Delta t) + \delta u_i^2 S^2(\Delta t) + \sigma_T^2 B_i^2 \Delta t^{2H} + \sigma_T^2 \varepsilon_i^2 \Delta t^{-1}$$

$$= \sigma_T^2 \varepsilon_i^2 \Delta t^{-1} + \sigma_T^2 (1 + \delta u_i^2 + B_i^2) \Delta t^{2H} + A^2 (1 + \delta u_i^2) \Delta t^2 \quad (25)$$

807 (the cross terms disappear because of the independence  
 808 assumption). The “ $\approx$ ” is used because we estimated the  
 809 ensemble average from the temporal averages on the indi-  
 810 vidual series so that for example,  $\left(\overline{\Delta G_H(\Delta t)^2}\right)^{1/2} = \Delta t^{2H}$

811 (see property 8, Sect. 3.1). Equation 25 shows that there are  
 812 three zones: a high frequency classical error measurement  
 813 term,  $\sigma_T^2 \varepsilon_i^2 \Delta t^{-1}$  a medium frequency missing data and scale  
 814 reduction term  $\sigma_T^2 (1 + \delta u_i^2 + B_i^2) \Delta t^{2H}$ , and a low frequency  
 815 scale reduction term  $A^2 (1 + \delta u_i^2) \Delta t^2$ . In “Appendix B”, we  
 816 show how the measurement model parameters can be esti-  
 817 mated from their structures functions and the structures  
 818 functions of the pairwise series differences (as in Figs. 2,  
 819 3). The results are that  $\delta u, B, \varepsilon$  are Gaussian random varia-  
 820 bles with estimated means and standard deviations ( $\mu, \sigma$ ):

$$821 \mu_{\delta u} = 0.114; \sigma_{\delta u} = 0.077$$

$$\mu_B = 0.347; \sigma_B = 0.175$$

$$\mu_\varepsilon = 0.132; \sigma_\varepsilon = 0.062 \quad (26)$$

822 Since the different random variables are somewhat cor-  
 823 related, using the above equation yields the “effective”  
 824 values needed for the simulations below. For complete-  
 825 ness, recall that we have already estimated  $H = -0.1, A =$   
 826  $(5.83 \pm 0.073) \times 10^{-4}$  K/month and  $\sigma_T = 0.142 \pm 0.01$  K  
 827 (Eqs. 20, 21).

828 In order to judge the implications, we can determine, the  
829 contribution of each of the three effects.

830 3.4.1 The scale reduction bias

831 This term is:

832 
$$\langle \Delta T(\Delta t)_{red}^2 \rangle^{1/2} = (\sigma_T^2 \mu_{\delta u}^2 \Delta t^{2H} + A^2 \mu_{\delta u}^2 \Delta t^2)^{1/2} \quad (27)$$

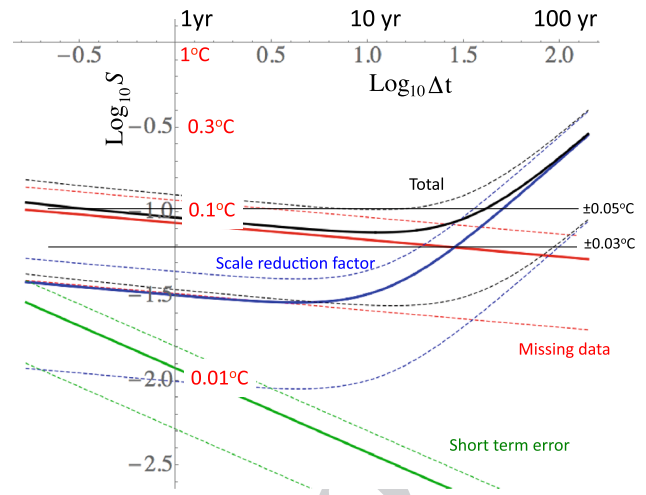
833 From Eqs. 26, 27, we have:  
834  $\langle \Delta T(\Delta t = 1 \text{ month})_{red}^2 \rangle^{1/2} = 0.020K$  (i.e.  $\pm 0.01$  K) (where  
835  $\Delta t$  are in units of months). Conversely, at the longest scales  
836 (133 years), we find  $\langle \Delta T(\Delta t = 133 \text{ yrs})_{red}^2 \rangle^{1/2} = 0.134K$   
837 ( $\pm 0.067$  K). In terms of the true earth temperature, from  
838 Eq. 22 we see that it implies a multiplicative bias of a factor  
839  $1 + \mu_{\delta u}$ , i.e.  $(\langle T_i(t) \rangle - T(t))/T(t) = \mu_{\delta u} \approx 11.4\%$  (recall that  
840  $T(t)$  is the true model temperature). The series to series variation  
841 in  $\delta u$ , is given by  $\sigma_{\delta u} = \pm 7.7\%$ ; it is significant. We can  
842 also check that it is plausible that it originates in variations in  
843 the effective space–time resolutions. To see this, recall that  
844 in Sect. 2.4 we argued that if two series differed in tempo-  
845 ral resolution by a factor  $\lambda_t$  and spatial resolution by a factor  
846  $\lambda_x$ , then the overall RMS scale reduction factor between  
847 the two would be  $e^{\mu_{\delta u}} \approx 1 + \mu_{\delta u} = \lambda_t^{-0.3} \lambda_x^{-0.2}$ . Therefore, the  
848 mean scale reduction factor  $\mu_{\delta u} = 0.114$  could be explained  
849 by perfect spatial resolution ( $\lambda_x = 1$ ) but inadequate temporal  
850 resolution  $\lambda_t \approx 0.7$ , by perfect temporal resolution ( $\lambda_t = 1$ )  
851 but inadequate spatial resolution  $\lambda_x \approx 0.6$ , or by some inter-  
852 mediate combination of imperfect spatial and temporal reso-  
853 lutions. These values correspond to differences in the effec-  
854 tive degree of temporal and spatial resolutions and they seem  
855 reasonable. This scale reduction factor most strongly affects  
856 the scale ranges dominated by anthropogenic effects. This  
857 can explain the observation (Fig. 1) that the global series dif-  
858 fers most strongly from each other in the recent (post  $\approx 1980$ )  
859 which is the period that has the strongest rate of anthropo-  
860 genic warming.

861 3.4.2 The bias due to missing data

862 We have:

863 
$$\langle \Delta T(\Delta t)_{miss}^2 \rangle^{1/2} = \sigma_T \mu_{\epsilon^2}^{1/2} \Delta t^H \quad (28)$$

864 so that at 1 month,  $\langle \Delta T(\Delta t = 1 \text{ month})_{miss}^2 \rangle^{1/2} = \pm 0.028K$   
865 whereas at 133 years  $\langle \Delta T(\Delta t = 133 \text{ yrs})_{miss}^2 \rangle^{1/2} = \pm 0.013K$   
866 put this in perspective, ignoring the low frequency  
867 anthropogenic term, the small short-range error term, and  
868 the scale reduction factor (this is a good approximation for  
869 resolutions  $\tau \approx 10$  years, see Fig. 6) then the missing data  
870 error variance is 15% of the true temperature variance:  
871  $\langle (T_\tau(t) - T_{i,\tau}(t))^2 \rangle / \langle T_\tau(t)^2 \rangle = \mu_{B^2} = 0.15$  (including the  
872 scale reduction factor increases this to  $\mu_{B^2} + \mu_{\delta u}^2 = 0.17$ ).



873 **Fig. 6** The structure functions of the various measurement errors  
874 with one standard deviation limits shown as *dashed lines* (corre-  
875 sponding the variation from one measurement series to another). The  
876 *blue curve* is the contribution of the scale reduction factor, the red is  
877 from missing data (slope =  $H = -0.1$ ) and the *green* is the short-range  
878 measurement error (slope  $-1/2$ ). The *black curve* is the sum of all the  
879 contributions. Notice that most of the contribution to the errors are  
880 from the scaling parts. These Haar structure functions have been multi-  
881 plied by a canonical factor of 2 so that the fluctuations will be closer  
882 to the anomalies (when decreasing) or differences (when increasing).  
883 Note that these show essentially the difference between the true earth  
884 temperature and the measurements; the difference between two dif-  
885 ferent measured series will have double the variances, the difference  
886 structure function should thus be increased by a further factor  $2^{1/2}$   
887 before comparison with Figs. 2, 3 or the figures below

873 Using  $\sigma_{B^2} = 0.104$  we see that the series to series variation  
874 about the 15% mean is about  $\pm 10\%$ .

875 3.4.3 The short-term error

876 We have:

877 
$$\langle \Delta T(\Delta t)_{error}^2 \rangle^{1/2} = \sigma_T \mu_{\epsilon^2}^{1/2} \Delta t^{-1/2} \quad (29)$$

878 so that at 1 month we have:  
879  $\langle \Delta T(\Delta t = 1 \text{ month})_{error}^2 \rangle^{1/2} = \pm 0.010K$  whereas for 133  
880 years, it is  $\langle \Delta T(\Delta t = 133 \text{ yrs})_{error}^2 \rangle^{1/2} = \pm 0.0003K$ . The  
881 total variance of the biases and errors is the sum of the  
882 three so that  $\langle \Delta T(\Delta t = 1 \text{ month})_{all}^2 \rangle^{1/2} = \pm 0.032K$  and  
883  $\langle \Delta T(\Delta t = 133 \text{ yrs})_{all}^2 \rangle^{1/2} = \pm 0.068K$ . The latter provides  
884 a good estimate of the centennial scale temperature errors  
885 relevant for evaluating the amplitude of the industrial epoch  
886 warming. Converting this to 90% certainty limits ( $\approx 1.6$   
887 standard deviations) we can say that with 90% certainty, for  
888 a given series, that the temperature change since 1880 is  
889 correct to within  $\pm 0.108$  °C.

890 It is useful to graphically assess the result by comparing  
891 the individual terms that contribute to the error and bias at

each scale  $\Delta t$ ; this is shown in Fig. 6. Starting with the short term error, we see that the smallest temporal resolution, it is roughly equal to the scale reduction factor but becomes quickly negligible at longer times. Until 10–20 years when the anthropogenic contribution becomes important, the errors are dominated by the missing data term, after that, by the scale reduction term. We can see that the total error is mostly in the range  $\pm 0.03$  to  $\pm 0.05$  °C, although it is a little higher at centennial scales. In the next subsection, we make stochastic simulations of the series and further evaluate the realism of the model.

### 3.5 Stochastic modelling the measurement process

We can now use the simulated “true” earth temperature (Fig. 5) with these parameters and Eq. 23 to create six simulations of the measured earth series. Figure 6 shows the result when they are presented in the same way as Fig. 1 (i.e. the grey “errors” are actually three standard deviations of the difference of the given series with respect to all the others). Since in this case the true temperature is known, we can also display the true errors (Fig. 7), which show that due to the variable scale reduction factors and variable missing data terms, some series have errors that are significantly different from the others. Figure 5 also shows the errors when the mean of the six simulations is used as the overall temperature estimate. From these simulations we can deduce some fairly simple statistics; for example at monthly resolutions, the RMS difference between the measured series and the truth is  $\pm(0.057 \pm 0.025)$  °C so that we can say that the series are “typically” in error by this amount (this is also

roughly the amplitude of the error curve with respect to the mean of the series shown at the bottom of Fig. 5). Also, the difference in the mean of each series with respect to the true mean (the bias in the temporal means) is:  $0.0087 \pm 0.040$  °C and the corresponding bias with respect to the mean of the six is:  $0 \pm 0.020$  °C (Fig. 8).

This means that if we choose a series at random, then there is 90% chance (1.6 standard deviations) that its bias is in the range  $-0.056$  to  $0.073$  °C and that its monthly RMS variation about its biased mean is in the range  $0.017$  to  $0.082$  °C. If we want to determine the absolute earth temperature, we can now choose the 20CR (the others only give anomalies). The preceding statistics indicate that for a given month its temperature will be in error by  $0.010 \pm 0.074$  °C (one standard deviation) so that with 90% certainty, the true monthly and globally averaged temperature is the range  $-0.109$  to  $0.127$  °C of the 20CR absolute temperature value for that month.

In order to test the model, we can use it to reconstruct the various structure function statistics discussed in Figs. 2, 3: the mean structure function  $\langle \Delta T(\Delta t)^2 \rangle^{1/2}$ , the mean difference structure function with respect to the mean  $\langle \Delta \delta T(\Delta t)^2 \rangle^{1/2}$ , the mean differences between pairs  $\langle \Delta \delta T(\Delta t)^2 \rangle^{1/2}$  and the standard deviation of the difference of the individual structure functions with respect to the mean of the others ( $\sigma_S(\Delta t) = \langle (S(\Delta t) - \langle S(\Delta t) \rangle)^2 \rangle^{1/2}$ ). The results are shown in Fig. 9; we can see that it well reproduces the empirical curves (Fig. 2); these are superposed for ease of comparison. Note that since the simulated series are analyzed in exactly the same way as the measurement series, that all nontrivial sampling and

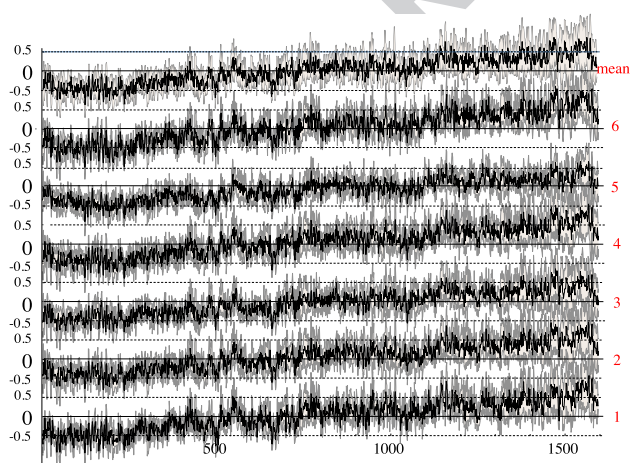


**Fig. 7** The six simulated earth temperature measurement series are shown using the same presentation as for the data in Fig. 1 i.e. with the grey indicating the three standard deviation limits of the excluded series. The top is the mean of all and the three standard deviation spread is the is due to spread of all the others

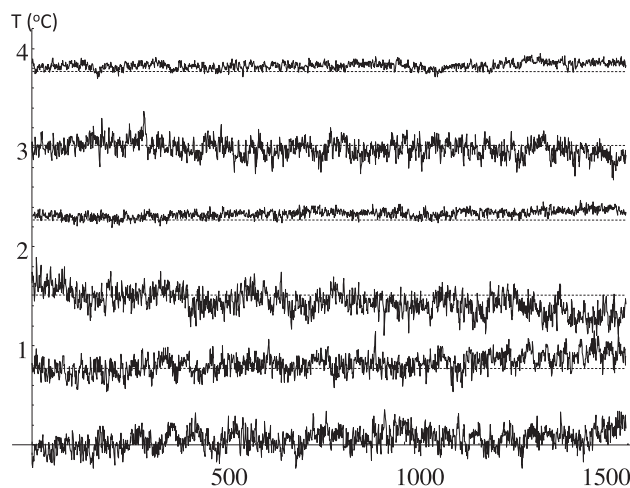


**Fig. 8** The absolute errors of the simulated measurement process, with each curve separated by 0.75 K for clarity. Perhaps the most obvious difference between the series is due to their differing scale reduction factors, these factors amplify all the errors by a given factor  $1 + \delta u$

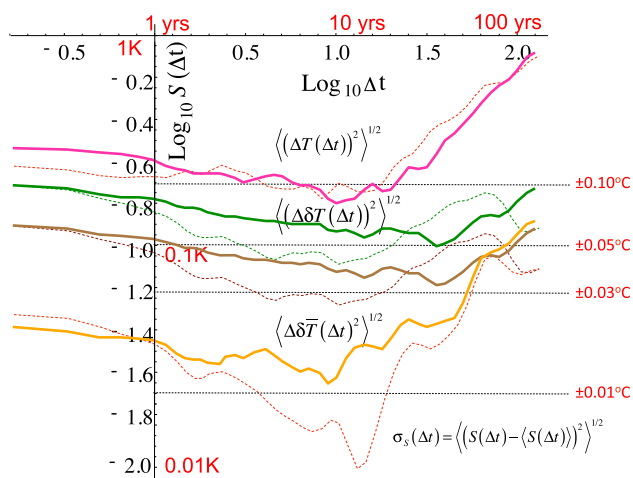
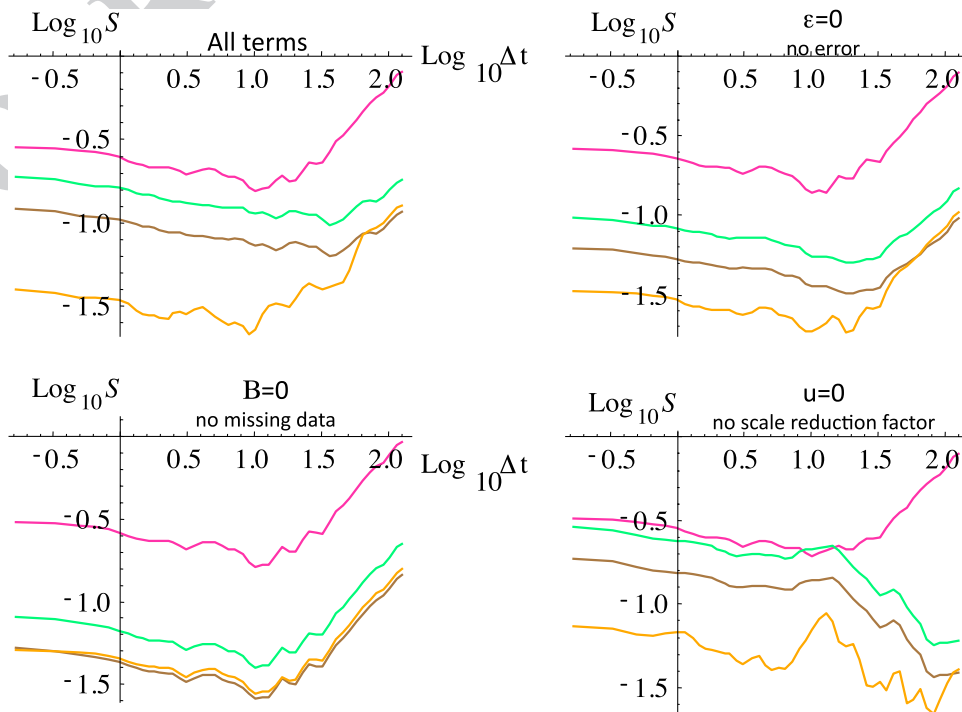


**Fig. 9** The dashed curves are the empirical curves reproduced from Fig. 2, the thick curves are the corresponding simulated curves using the simulations from Fig. 3

analysis issues are accounted for in the simulations so that the simulation—data agreement is highly significant. Another way of evaluating these effects is shown in Fig. 10. This displays the same series of structure functions and structure functions of differences that were shown in Fig. 9, except that we systematically remove one of the terms so as to gauge its effect on the statistics. The upper right graph shows that although the short range error term is small, that it nevertheless gives a noticeable contribution

**Fig. 10** The various contribution to  $\langle \Delta T(\Delta t)^2 \rangle^{1/2}$  (pink, top),  $\langle \Delta \delta T(\Delta t)^2 \rangle^{1/2}$  (green, 2nd from top),  $\langle \Delta \delta \bar{T}(\Delta t)^2 \rangle^{1/2}$  (brown, third from top) and  $\sigma_s$  (orange, bottom) with statistics averaged over the six simulated series  $\langle (\Delta T(\Delta t)^2)^{1/2} \rangle$ ,  $\langle \Delta \delta T(\Delta t)^2 \rangle^{1/2}$ ,  $\langle \Delta \delta \bar{T}(\Delta t)^2 \rangle^{1/2}$ ,  $\sigma_s$ , and pairs of differences  $\langle (\Delta \delta T(\Delta t)^2)^{1/2} \rangle$ . The upper left graph shows the result with all three error terms present, the upper right when the short term error is removed ( $\epsilon=0$ ), lower left when the missing data term is removed ( $B=0$ ) and lower right after the scale reduction factor is removed ( $\delta u=0$ )

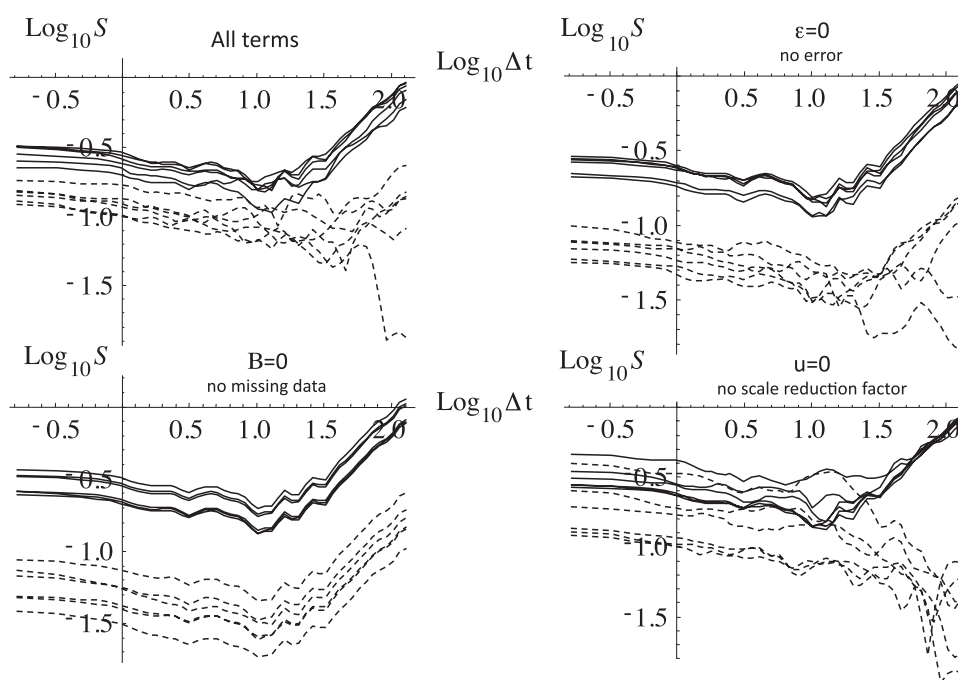


especially to the differences  $\langle \Delta \delta T(\Delta t)^2 \rangle^{1/2}$ ,  $\langle \Delta \delta \bar{T}(\Delta t)^2 \rangle^{1/2}$  (green and brown respectively). With no missing data (bottom left), the difference curves are (unrealistically) very close to each other. Finally (lower right), we see that the scale reduction factor is essential for explaining the statistics at long  $\Delta t$ . Rather than displaying simply the means of the six simulations, we can also show the statistics of the individual realizations that were used in calculating the means (Fig. 11); we see that the series to series variability is fairly realistic (c.f. Fig. 3).

### 4 Conclusions

Accurate global scale temperature estimates are important in many applications, especially global warming. Deviations of estimated global scale surface temperatures from the true global mean (i.e. errors plus biases) arise not only from human induced inhomogeneities but also because of objective difficulties in determining (spatial) temperature fields from point-like station values. The difficulties are fundamental since the temperature field has nonclassical space-time statistical behaviours (especially scaling and intermittency), and the measuring networks are also sparse (fractal) in both time and in space (they have “holes” at all scales). Rather than attempting to directly quantify the uncertainty with the help of classical statistical assumptions and models, we therefore exploited the fact that a

**Fig. 11** Similar to Fig. 10 for  $\langle \Delta T(\Delta t)^2 \rangle^{1/2}$  and  $\langle \Delta \delta \bar{T}(\Delta t)^2 \rangle^{1/2}$  except that the results for each of the six simulated measurement terms are shown separately. The structure functions  $\langle \Delta T(\Delta t)^2 \rangle^{1/2}$  (thick, top), and differences with respect to the mean  $\langle \Delta \delta \bar{T}(\Delta t)^2 \rangle^{1/2}$  (bottom, dashed) for each of the six individual realizations used shown in Fig. 6 and used in Figs. 9, 10. Compare this to Fig. 3 for the data



987 half dozen or more series have been produced, each using  
 988 somewhat different data and methodologies. Before mak-  
 989 ing specific assumptions about the errors and biases in the  
 990 data and attempting to directly quantify them with respect  
 991 to the real world, we first ask (Sect. 2) how well do differ-  
 992 ent approaches agree with each other as functions of time  
 993 scale (what are the relative errors)?

994 In order to isolate the deviations at different time scales  
 995 we estimated fluctuations and determined their average root  
 996 mean square values from two months to 133 years (from  
 997 1880 to 2012). Perhaps the most obvious conclusion was  
 998 that although each series was quite similar to the others—  
 999 and this includes one that was based on only monthly SST  
 1000 and surface pressure observations (the 20CR)—that *even*  
 1001 *at long time scales differences between the series did not*  
 1002 *converge*. This is surprising since classical theory shows  
 1003 that for short range correlated errors (e.g. AR(1) processes  
 1004 or kindred processes that are essentially Gaussian white  
 1005 noises at long enough time scales) their RMS differences  
 1006 diminish as  $\Delta t^{-1/2}$ . Instead of this, from months to centen-  
 1007 nial scales, the RMS fluctuations stayed nearly constant,  
 1008 mostly between  $\approx \pm 0.03^\circ\text{C}$  and  $\pm 0.05^\circ\text{C}$  (one standard  
 1009 deviations); they slightly increased at long times, Figs. 2,  
 1010 3. Since the variability at scales  $> \approx 10$  years is dominated  
 1011 by the anthropogenic forcing, this is a direct estimate of the  
 1012 accuracy with which the latter can be estimated. Also sig-  
 1013 nificant is the finding that the *statistics* of the fluctuations  
 1014 can be estimated with much higher relative accuracy (e.g.  
 1015 between 3 and 10 years to better than  $\pm 0.0005^\circ\text{C}$ ).

1016 The fact that the differences between the series have  
 1017 nearly constant deviations—*independent of the time*

scale—demonstrates the existence long-range statistical  
 dependencies in the series errors and biases that are out-  
 side conventional geostatistical uncertainty assumptions  
 requires the development of new methodologies.

1022 In order to go beyond relative errors (Sect. 2), so as to  
 1023 estimate absolute errors (Sect. 3), we need models of both  
 1024 the earth's true temperature and of the measurement pro-  
 1025 cess itself. For the former, we assumed a combination of  
 1026 natural variability modelled by a scaling, fractional Gaus-  
 1027 sian noise (fGn) process combined with a linear trend rep-  
 1028 resenting the anthropogenic warming. While the former is the  
 1029 simplest scaling model (it is nonintermittent), the latter is  
 1030 an approximation to an anthropogenic contribution (in real-  
 1031 ity, the latter is much more linear as a function of the  $\text{CO}_2$   
 1032 radiative forcing than as a function of time).

1033 For the measurement errors, although we included a  
 1034 classical short range error term, in order to account for the  
 1035 dominant high and low frequency errors, we need two new  
 1036 sources of error: we introduced both missing data and scale  
 1037 reduction factors. The error due to missing data must have  
 1038 the same type of temporal statistics as the nonmissing data,  
 1039 so that it was also modelled as an fGn process. However, as  
 1040 fGn processes are averaged to lower and lower resolutions,  
 1041 their amplitudes diminish (this affects all the frequencies)  
 1042 so that by itself, missing data is not sufficient for explain-  
 1043 ing the low frequency errors. For the latter, we relied on  
 1044 the observation (Sect. 2.4) that the temperature anomalies  
 1045 are highly sensitive to their space–time resolutions: in both  
 1046 space and in time, fluctuations systematically decrease in  
 1047 amplitude with increasing scale (in roughly scaling, power  
 1048 law manners). This means that if a series is insufficiently

1049 averaged—in space and/or in time—then its effective resolu- 1101  
 1050 tion will be different from the nominal resolution (here, 1102  
 1051 one month, globally averaged). This scale/resolution effect 1103  
 1052 is multiplicative so that it affects all frequencies. Follow- 1104  
 1053 ing the hydrology literature’s analogous “areal reduction 1105  
 1054 factor” (due to spatial resolution effects), this more general 1106  
 1055 (space–time) effect is a “scale reduction factor”.

1056 In order to test the model we need to estimate its param- 1107  
 1057 eters; two for the earth model (the amplitude of the natu- 1108  
 1058 ral variability and the anthropogenic trend), and three for 1109  
 1059 the measurement process:  $\epsilon$ ,  $B$ ,  $\delta u$  (the amplitudes of the 1110  
 1060 short term error, the missing data and the scale reduction 1111  
 1061 factor). Since the measurement process is stochastic with 1112  
 1062 each series characterized by a different triplet of amplitudes 1113  
 1063 we only need their statistics (assumed to be Gaussian, we 1114  
 1064 need their means and standard deviations). We showed 1115  
 1065 how to make robust parameter estimates using structure 1116  
 1066 function analyses of the  $6 \times 5/2 = 15$  pairs of series differ- 1117  
 1067 ences. We found for example that the measurement error 1118  
 1068 was about  $\pm 0.01$  K at one month decreasing rapidly for 1119  
 1069 longer times. That the missing data term was dominant and 1120  
 1070 contributed about 15% to the variance of the temperature at 1121  
 1071 all resolutions up to about 10–20 years (the series to series 1122  
 1072 variability is about 10% around this mean value). Beyond 1123  
 1073 this, ( $\Delta t \approx > 10$ –20 years) the scale reduction factor was 1124  
 1074 dominant, so that temperature anomalies (due to inadequate 1125  
 1075 space–time averaging) were on average about 11% too large 1126  
 1076 with a series to series variability of about 8% around this 1127  
 1077 value.

1078 Finally, using the estimated parameters, we made sto- 1128  
 1079 chastic simulations of both the “true” earth temperature and 1129  
 1080 the measurement process (including all the sampling issues 1130  
 1081 in the statistical analysis) and showed that all the fluctua- 1131  
 1082 tion statistics as functions of time—including the pairwise 1132  
 1083 difference fluctuations—were very close to the observa- 1133  
 1084 tions so that the model quantitatively accounts for all the 1134  
 1085 differences between the series and all sampling issues. We 1135  
 1086 thus have confidence that we have an accurate estimate of 1136  
 1087 the absolute temperature errors, and—as for the relative 1137  
 1088 errors—these are generally in the range  $\pm 0.03$  to  $\pm 0.05$  K 1138  
 1089 over almost all the range of time scales (month to 133 1139  
 1090 years). More precisely, at monthly scales, we found that for 1140  
 1091 a given month and series, its temperature will be in error 1141  
 1092 by  $0.010 \pm 0.074$  °C (one standard deviation) so that with 1142  
 1093 90% certainty, the true monthly and globally averaged tem- 1143  
 1094 perature is the range  $-0.109$  to  $0.127$  °C of the temperature 1144  
 1095 value for that month. At centennial scales, we estimated 1145  
 1096 that with 90% certainty, that the corresponding temperature 1146  
 1097 change since 1880 is correct to within  $\pm 0.108$  °C (i.e. about 1147  
 1098 10% of the industrial epoch warming).

1099 In order to give a satisfactory estimate of the accuracy of 1148  
 1100 global temperatures, we showed that a new approach was

needed and we suggested a simple stochastic temperature and 1101  
 measurement model based on the observed scaling of global 1102  
 temperatures. This approach can readily be extended in a 1103  
 number of directions for quantifying measurement uncertain- 1104  
 ties. For example, for the temperature, it could be extended 1105  
 to varying spatial resolutions, indeed the relative accuracy 1106  
 method—using pairwise series differences but at  $5^\circ \times 5^\circ$  reso- 1107  
 lution—has already been applied to global precipitation (de 1108  
 Lima and Lovejoy 2015). In future it may also be applied to 1109  
 determining the accuracy of pre-industrial multiproxies. 1110

**Acknowledgements** The author thanks R. Hébert, L. del Rio Ama- 1111  
 dor and David Clarke for useful discussions. This work was unfunded, 1112  
 there were no conflicts of interest. The data were downloaded from 1113  
 the publically accessible sites to be found in the corresponding refer- 1114  
 ences (first paragraph, Sect. 2). 1115

**Appendix A: some useful properties of fractional Gaussian noise** 1116  
 1117

In this appendix, we give a brief summary of some use- 1118  
 ful properties of fGn; a longer review is given in (Lovejoy 1119  
 et al. 2015b) and a full mathematical exposé in (Biagini 1120  
 et al. 2008). The standard (“s”) fGn process  $G_H^{(s)}(t)$  with 1121  
 parameter  $H$ , can be defined as: 1122

$$G_H^{(s)}(t) = \frac{c_H}{\Gamma(1/2+H)} \int_{-\infty}^t (t-t')^{-(1/2-H)} \gamma(t') dt'; \quad -1 < H < 0 \quad (30)$$

$\gamma(t)$  is a unit Gaussian “ $\delta$  correlated” white noise with 1124  
 $\langle \gamma \rangle = 0$  and: 1125

$$\langle \gamma(t)\gamma(t') \rangle = \delta(t-t') \quad (31)$$

where “ $\delta$ ” is the Dirac function. The constant  $c_H$  is a con- 1127  
 stant chosen so as to make the expression for the statistics 1128  
 particularly simple, see below. It may be useful to note that 1129  
 fGn is related by differentiation to the more familiar frac- 1130  
 tional Brownian motion (fBm) process. We can see by 1131  
 inspection of Eq. 16 that  $G_H^{(s)}(t)$  is statistically stationary 1132  
 and by taking ensemble averages of both sides of Eq. 16 we 1133  
 see that the mean vanishes:  $\langle G_H^{(s)}(t) \rangle = 0$ . When  $H = -1/2$ , 1134  
 the process  $G_{-1/2}^{(s)}(t)$  is simply a Gaussian white noise. 1135

Now, take the average of  $G_H$  over  $\tau$ ; the “ $\tau$  resolution 1136  
 anomaly fluctuation”:

$$G_{H,\tau}^{(s)}(t) = \frac{1}{\tau} \int_{t-\tau}^t G_H^{(s)}(t') dt' \quad (32)$$

If  $c_H$  is now chosen such that:

$$c_H = \left( \frac{\pi}{2\cos(\pi H)\Gamma(-2H-2)} \right)^{1/2} \quad (33)$$

then we have:

$$\langle G_{H,\tau}^{(s)}(t)^2 \rangle = \tau^{2H}; \quad -1 < H < 0 \quad (34)$$

This shows that a fundamental property of fGn is that in the small scale limit ( $\tau \geq 0$ ), the variance diverges and  $H$  is scaling exponent of the root mean square (RMS) value. This singular small scale behaviour is responsible for the strong power law resolution effects in fGn. Since  $\langle G_H^{(s)}(t) \rangle = 0$ , sample functions  $G_{H,\tau}(t)$  fluctuate about zero with successive fluctuations tending to cancel each other out; this is the hallmark of macroweather.

A comment on the parameter  $H$  is now in order. In treatments of fBm, it is usual to use the parameter  $H$  confined to the unit interval i.e. to characterize the scaling of the increments of fBm. However, fBm (and fGn) are very special scaling processes, and even in low intermittency regimes such as macroweather—they are at best approximate models of reality. Therefore, it is better to define  $H$  more generally as the fluctuation exponent (Eq. 9); with this definition  $H$  is also useful for more general (multifractal) scaling processes although the common interpretation of  $H$  as the ‘‘Hurst exponent’’ is only valid for fBm in the usual fGn literature, the parameter  $H$  is the fluctuation exponent of its integral, fBm, i.e. it is larger by unity than that used here.

### Anomalies

An anomaly is the average deviation from the long term average and since  $\langle G_H^{(s)}(t) \rangle = 0$ , the anomaly fluctuation over interval  $\Delta t$  is simply  $G_H$  at resolution  $\Delta t$  rather than  $\tau$ :

$$\left( \Delta G_{H,\tau}^{(s)}(\Delta t) \right)_{anom} = \frac{1}{\Delta t} \int_{t-\Delta t}^t G_{H,\tau}^{(s)}(t') dt' = \frac{1}{\Delta t} \int_{t-\Delta t}^t G_H^{(s)}(t') dt' = G_{H,\Delta t}^{(s)}(t); \quad \Delta t > \tau \quad (35)$$

Hence using Eq. 34:

$$\left\langle \left( \Delta G_{H,\tau}^{(s)}(\Delta t) \right)_{anom}^2 \right\rangle = \Delta t^{2H}; \quad -1 < H < 0 \quad (36)$$

### Differences

In the large  $\Delta t$  limit we have:

$$\left\langle \left( \Delta G_{H,\tau}^{(s)}(\Delta t) \right)_{diff}^2 \right\rangle \approx 2\tau^{2H} \left( 1 - (H+1)(2H+1) \left( \frac{\Delta t}{\tau} \right)^{2H} \right); \quad \Delta t \gg \tau \quad (37)$$

Since  $H < 0$ , the differences asymptote to the value  $2\tau^{2H}$  (double the variance). Notice that since  $H < 0$ , the differences are not scaling with  $\Delta t$ .

### Haar fluctuations

For the Haar fluctuation we obtain:

$$\left\langle \left( \Delta G_{H,\tau}^{(s)}(\Delta t) \right)_{Haar}^2 \right\rangle = 4\Delta t^{2H} (2^{-2H} - 1); \quad \Delta t \geq 2\tau \quad (38)$$

this scales as  $\Delta t^{2H}$  and does not depend on the resolution  $\tau$  (Lovejoy et al. 2015a).

Since we will use Haar fluctuations throughout, it is convenient to define the fGn  $G_H(t)$  with a nonstandard normalization replacing the constant  $c_H$  in Eq. 30 by  $c'_H$ :

$$c'_H = \frac{c_H}{2\sqrt{2^{-2H} - 1}} \quad (39)$$

With this we can define  $G_{H,\tau} = \frac{G_{H,\tau}^{(s)}}{2\sqrt{2^{-2H} - 1}}$  so that:

$$\left\langle \left( \Delta G_{H,\tau}(\Delta t) \right)_{Haar}^2 \right\rangle = \Delta t^{2H}; \quad \Delta t \geq 2\tau. \quad (40)$$

### Appendix B: estimating the parameters of the measurement model

In this appendix, we describe how we estimated the statistics of the amplitudes of the measurement series noises ( $\delta u$ ,  $B$ ,  $\varepsilon$ , for the scale reduction factor, missing data and conventional measurement error respectively).

The idea is to use second order structure functions (Sect. 3), however from structure functions we can only estimate the squared quantities ( $\delta u^2$ ,  $B^2$ ,  $\varepsilon^2$ ). We therefore used an easily verifiable result, valid for a Gaussian random variable  $x$ :

$$\begin{aligned} \mu_x &= \pm \left( \mu_{x^2} - \frac{\sigma_{x^2}^2}{2} \right)^{1/4} \\ \sigma_x &= \left( \mu_{x^2} - \mu_x^2 \right)^{1/2} \end{aligned} \quad (41)$$

where  $\mu_x$ ,  $\sigma_x$  are respectively the means and standard deviations of  $x$  and  $\mu_{x^2}$ ,  $\sigma_{x^2}$  of  $x^2$ . Finally, the sign of  $\mu_x$  is not determined. In the case of  $B$ ,  $\varepsilon$ , this is unimportant since they are multiplied by sign symmetric random functions so that without loss of generality we can take  $\mu_B > 0$ ,  $\mu_\varepsilon > 0$ , but for  $\delta u$ , there is an ambiguity. However, since presumably the series are insufficiently averaged, we expect  $\delta u > 0$  so that below, we use the plus sign.

The error in the squared fluctuation variance at each scale  $\Delta t$  is therefore:



1210

$$\begin{aligned} S_i^2(\Delta t) - S^2(\Delta t) &= \delta u_i^2 S^2(\Delta t) + \sigma_T^2 B_i^2 \Delta t^{2H} + \sigma_T^2 \varepsilon_i^2 \Delta t^{-1} \\ &= \sigma_T^2 \varepsilon_i^2 \Delta t^{-1} + \sigma_T^2 (\delta u_i^2 + B_i^2) \Delta t^{2H} + A^2 \delta u_i^2 \Delta t^2 \end{aligned} \quad (42)$$

1211 where  $S(\Delta t)$  is the ensemble averaged true earth structure  
1212 function (see Eq. 25). Since at large  $\Delta t$  the  $\Delta t^2$  term is  
1213 dominant, regression of this equation against  $\Delta t^2$  can con-  
1214 veniently be used to estimate  $\mu_{\delta u} = 0.114$  and  $\sigma_{\delta u} = 0.077$ .  
1215 However the other terms are smaller and to obtain robust  
1216 estimates it is advantageous to consider the pairwise differ-  
1217 ences as in Figs. 2, 3. Since there are six series, we have  
1218  $6 \times 5/2 = 15$  pairs, giving us substantially more statistics  
1219 with which to estimate the missing data and error ampli-  
1220 tudes  $B_i, \varepsilon_i$  of the  $i$ th series (here, the index  $i$  runs from 1 to  
1221 6). Therefore, consider the differences between the  $i$ th and  
1222  $j$ th series of measurements:

$$\delta T_{ij}(t) = \sigma_T \delta u_{ij} G_H^{(0)}(t) + A \delta u_{ij} t + \sigma_T B_{ij} G_H^{(ij)}(t) + \sigma_T \varepsilon_{ij} G_{-1/2}^{(ij)}(t) \quad (43)$$

1224 where  $\delta u_{ij}^2 = \delta u_i^2 + \delta u_j^2$  and we have used the mathematical  
1225 result:

$$\begin{aligned} B_{ij} G_H^{(ij)}(t) &\stackrel{d}{=} B_i G_H^{(i)}(t) - B_j G_H^{(j)}(t); \quad B_{ij}^2 = B_i^2 + B_j^2 \\ \varepsilon_{ij} G_{-1/2}^{(ij)}(t) &\stackrel{d}{=} \varepsilon_i G_{-1/2}^{(i)}(t) - \varepsilon_j G_{-1/2}^{(j)}(t); \quad \varepsilon_{ij}^2 = \varepsilon_i^2 + \varepsilon_j^2 \end{aligned} \quad (44)$$

1227 where “ $\stackrel{d}{=}$ ” indicates equality in probability distributions  
1228 (so that  $G_H^{(ij)}(t) \stackrel{d}{=} G_H^{(i)}(t) - G_H^{(j)}(t)$ ). These results follow since  
1229 sums and differences of independent Gaussian variables are  
1230 also Gaussian and their variances add.

1231 Therefore the fluctuations in the differences are:

$$\begin{aligned} \delta \Delta T_{ij}(\Delta t) &= \sigma_T \delta u_{ij} \Delta G_H^{(0)}(\Delta t) + A \delta u_{ij} \Delta t + \sigma_T B_{ij} \Delta G_H^{(ij)}(\Delta t) \\ &\quad + \sigma_T \varepsilon_{ij} \Delta G_{-1/2}^{(ij)}(\Delta t) \end{aligned} \quad (45)$$

1233 With this, squaring and averaging, we obtain for the cor-  
1234 responding squared structure function:

$$S_{ij}^2(\Delta t) = \overline{\delta \Delta T_{ij}(\Delta t)^2} = \sigma_T^2 \varepsilon_{ij}^2 \Delta t^{-1} + \sigma_T^2 (\delta u_{ij}^2 + B_{ij}^2) \Delta t^{2H} + A^2 \delta u_{ij}^2 \Delta t^2 \quad (46)$$

1236 We can now estimate the parameters by regression of  
1237  $S_{ij}^2(\Delta t)$  on the fifteen  $i, j$  pairs of difference structure func-  
1238 tions against  $\Delta t^{-1}, \Delta t^{2H}$  (with  $H = -0.1$ ) and  $\Delta t^2$ . To make  
1239 the problem numerically more robust, we used the fact that  
1240 the trend  $A$  was estimated earlier from regressions on the  
1241 individual series  $T_i(t)$ . Similarly, for each of the six  $S_i(\Delta t)^2$   
1242 functions, we estimated the trends  $A^2 \delta u_i^2$ ; using the esti-  
1243 mates for  $A$  this leads to estimates of  $\mu_{\delta u}, \sigma_{\delta u}, \delta u_{ij}^2 = \delta u_i^2 +$   
1244  $\delta u_j^2$ . These trends were then removed to obtain the (quad-  
1245 ratically) detrended difference structure function  
1246  $S_{ij, \text{det}}^2(\Delta t) = \sigma_T^2 \varepsilon_{ij}^2 \Delta t^{-1} + \sigma_T^2 (\delta u_{ij}^2 + B_{ij}^2) \Delta t^{2H}$ ; when  
1247 regressed against  $\Delta t^{-1}, \Delta t^{2H}$ , these gave robust estimates of

the prefactors  $\sigma_T^2 \varepsilon_{ij}^2$  and  $\sigma_T^2 (\delta u_{ij}^2 + B_{ij}^2)$ . Combined with the  
trend based estimates of  $\delta u_{ij}^2$ , we thus obtain 15 estimates  
for each of the random variables,  $\varepsilon_{ij}^2, B_{ij}^2$ . If we assume that

the parameters are independent identically distributed ran-  
dom variables then Eq. 38 shows that:

$$\begin{aligned} B_{ij}^2 &\stackrel{d}{=} 2B_i^2 \stackrel{d}{=} 2B_j^2 \\ \varepsilon_{ij}^2 &\stackrel{d}{=} 2\varepsilon_i^2 \stackrel{d}{=} 2\varepsilon_j^2 \end{aligned} \quad (47)$$

Therefore, we use the estimates of  $\varepsilon_{ij}^2, B_{ij}^2$  to obtain esti-  
mates of the statistics of  $\varepsilon_i^2, B_i^2$ , and then from Eq. 35, by  
assuming the variables are Gaussian, we obtain estimates  
for the means and standard deviations of  $\varepsilon_i, B_i$ . For com-  
pleteness, we give the means and standard deviations of  
 $\delta u_i$ , obtained from  $S_i(\Delta t)$  as explained earlier.

$$\begin{aligned} \mu_{\delta u} &= 0.114; \quad \sigma_{\delta u} = 0.077 \\ \mu_B &= 0.347; \quad \sigma_B = 0.175 \\ \mu_\varepsilon &= 0.132; \quad \sigma_\varepsilon = 0.062 \end{aligned} \quad (48)$$

(due to the ambiguity in the sign, we did not take the square  
root of Eq. 41 to more directly yield  $B_i, \varepsilon_i$ ). Since the dif-  
ferent random variables are somewhat correlated, using the  
above equation yields the “effective” values needed for the  
simulations below. For completeness, recall that we have  
already estimated  $H = -0.1, A = (5.83 \pm 0.073) \times 10^{-4}$  K/  
month and  $\sigma_T = 0.142 \pm 0.01$  K (Eqs. 20, 21).

## References

- Bendjoudi, H., Hubert, P., Schertzer, D., Lovejoy, S. (1997), Interprétation multifractale des courbes intensité-durée-fréquence des précipitations, Multifractal point of view on rainfall intensity-duration-frequency curves, C.R.-A.-S., (Sciences de la terre et des planetes/Earth and Planetary Sciences). 325:323–326
- Biagini F, Hu Y, Øksendal B, Zhang T (2008) Stochastic Calculus for Fractional Brownian Motion and Applications. Springer-Verlag, London
- Brohan P, Kennedy JJ, Harris I, S. F. B. Tett, Jones PD (2006) Uncertainty estimates in regional and global observed temperature changes: a new dataset from 1850. J Geophys Res 111:D12106 doi:10.1029/2005JD006548
- Bunde A, Eichner JF, Havlin S, Koscielny-Bunde E, Schellnhuber HJ, Vyushin D (2004) Comment on “scaling of atmosphere and ocean temperature correlations in observations and climate models”. Phys Rev Lett 92:039801–039801
- Compo GP et al (2011) The twentieth century reanalysis project. Quarterly J Roy Meteorol Soc 137:1–28 doi:10.1002/qj.776
- Compo GP, Sardeshmukh PD, Whitaker JS, Brohan P, Jones PD, McColl C (2013) Independent confirmation of global land warming without the use of station temperatures. Geophys Res Lett 40:3170–3174 doi:10.1002/grl.50425
- Cowan K, Way RG (2014) Coverage bias in the HadCRUT4 temperature series and its impact on recent temperature trends. Q J R Meteorol Soc 140:1935–1944. doi:10.1002/qj.2297
- de Lima MIP, Lovejoy S (2017) Macroweather precipitation variability up to global and centennial scales. Wat Resour Res

- 1296 Diamond HJ et al (2013) US climate reference network after one decade of operations: status and assessment. *Bull Amer Meteor Soc* 94:485–498 doi:[10.1175/BAMS-D-12-00170.1](https://doi.org/10.1175/BAMS-D-12-00170.1)
- 1297
- 1298
- 1299 Efstathiou MN, Varotsos CA (2010) On the altitude dependence of the temperature scaling behaviour at the global troposphere. *Int J Remote Sens* 31(2):343–349
- 1300
- 1301
- 1302 Franzke C (2012) Nonlinear trends, long-range dependence and climate noise properties of temperature. *J Clim* 25:4172–4183. doi:[10.1175/JCLI-D-11-00293.1](https://doi.org/10.1175/JCLI-D-11-00293.1)
- 1303
- 1304 Hansen J, Ruedy R, Sato M, Lo K (2010) Global surface temperature change. *Rev Geophys* 48:RG4004 doi:[10.1029/2010RG000345](https://doi.org/10.1029/2010RG000345)
- 1305
- 1306 Hausfather Z, Cowtan K, Clarke DC, Jacobs P, Richardson M, Rohde R (2017) Assessing recent warming using instrumentally-homogeneous sea surface temperature records. *Sci Adv*
- 1307
- 1308 Karl TR, Arguez A, Huang B, Lawrimore JH, McMahon JR, Menne MJ, Peterson TC, Vose RS, Zhang H-M (2015) Possible artifacts of data biases in the recent global surface warming hiatus. *Sci Expr* 1–4 doi:[10.1126/science.aaa5632](https://doi.org/10.1126/science.aaa5632)
- 1309
- 1310 Kennedy JJ, Rayner NA, Smith RO, Saunby M, Parker DE (2011) Reassessing biases and other uncertainties in sea-surface temperature observations measured in situ since 1850 part 2: biases and homogenisation. *J Geophys Res* 116:D14104. doi:[10.1029/2010JD015220](https://doi.org/10.1029/2010JD015220)
- 1311
- 1312 Kondratyev KY, Varotsos C (1995) Atmospheric greenhouse effect in the context of global climate change. *Il Nuovo Cimento C* 18(2):123–151
- 1313
- 1314 Lovejoy S (2013) What is climate? *EOS* 94(1)
- 1315
- 1316 Lovejoy S (2014) Scaling fluctuation analysis and statistical hypothesis testing of anthropogenic warming. *Clim Dyn* 42:2339–2351. doi:[10.1007/s00382-014-2128-2](https://doi.org/10.1007/s00382-014-2128-2)
- 1317
- 1318 Lovejoy S (2015) A voyage through scales, a missing quadrillion and why the climate is not what you expect. *Climate Dyn* 44:3187–3210 doi:[10.1007/s00382-014-2324-0](https://doi.org/10.1007/s00382-014-2324-0)
- 1319
- 1320 Lovejoy S, de Lima MIP (2015) The joint space-time statistics of macroweather precipitation, space-time statistical factorization and macroweather models. *Chaos* 25:075410. doi:[10.1063/1.4927223](https://doi.org/10.1063/1.4927223)
- 1321
- 1322 Lovejoy S, Schertzer D (1986) Scale invariance, symmetries, fractals and stochastic simulations of atmospheric phenomena. *Bulletin of the AMS* 67:21–32
- 1323
- 1324 Lovejoy S, Schertzer D (2010) Towards a new synthesis for atmospheric dynamics: space-time cascades. *Atmos Res*. doi:[10.1016/j.atmosres.2010.01.004](https://doi.org/10.1016/j.atmosres.2010.01.004)
- 1325
- 1326 Lovejoy S, Schertzer D (2012a). Low frequency weather and the emergence of the Climate. In: Sharma AS, Bunde A, Baker DN, Dimri VP (eds) *Extreme events and natural hazards: the complexity perspective*, AGU monographs, Washington DC, pp. 231–254
- 1327
- 1328 Lovejoy S, Schertzer D (2012b) Haar wavelets, fluctuations and structure functions: convenient choices for geophysics. *Nonlinear Proc Geophys* 19:1–14. doi:[10.5194/npg-19-1-2012](https://doi.org/10.5194/npg-19-1-2012)
- 1329
- 1330 Lovejoy S, Schertzer D (2013) *The Weather and Climate: Emergent Laws and Multifractal Cascades*. Cambridge University Press, Cambridge
- 1331
- 1332 Lovejoy S, Schertzer D, Ladoy P (1986) Fractal characterisation of inhomogeneous measuring networks. *Nature* 319:43–44
- 1333
- 1334 Lovejoy S, Schertzer D, Varon D (2013a) How scaling fluctuation analyses change our view of the climate and its models (Reply to R. Pielke sr.: Interactive comment on “Do GCM’s predict the climate... or macroweather?” by S. Lovejoy et al.). *Earth Syst Dynam Discuss* 3:C1–C12
- 1335
- 1336 Lovejoy S, Schertzer D, Varon D (2013b) Do GCM’s predict the climate... or macroweather? *Earth Syst Dynam* 4:1–16. doi:[10.5194/esd-4-1-2013](https://doi.org/10.5194/esd-4-1-2013)
- 1337
- 1338
- 1339 Lovejoy S, del Rio Amador L, Hébert R (2015a) The Scaling LNear Macroweather model (SLIM): using scaling to forecast global scale macroweather from months to decades. *Earth System Dyn Disc* 6:489–545 doi:[10.5194/esdd-6-489-2015](https://doi.org/10.5194/esdd-6-489-2015)
- 1340
- 1341
- 1342 Lovejoy S, del Rio Amador L, Hébert R (2015b) The ScaLIng Macroweather Model (SLIMM): using scaling to forecast global-scale macroweather from months to Decades. *Earth Syst Dynam* 6:1–22. doi:[10.5194/esd-6-1-2015](https://doi.org/10.5194/esd-6-1-2015)
- 1343
- 1344 Lovejoy S, del Rio Amador L, Hébert R, de Lima I (2016) Giant natural fluctuation models and anthropogenic warming. *Geophys Res Lett*. doi:[10.1002/2016GL070428](https://doi.org/10.1002/2016GL070428)
- 1345
- 1346 Lovejoy S, del Rio Amador L, Hébert R (2017) Harnessing butterflies: theory and practice of the Stochastic Seasonal to Interannual Prediction System (StocSIPS). In: Tsonis AA (ed) *Nonlinear Advances in Geosciences*. Springer Nature
- 1347
- 1348 Mann ME (2011) On long range dependence in global surface temperature series. *Clim Change* 107:267–276
- 1349
- 1350 Mazzarella A, Tranfaglia G (2000) Fractal characterisation of geophysical measuring networks and its implication for an optimal location of additional stations: an application to a rain-gauge network. *Theor Appl Climatology* 65:157–163 doi:[10.1007/s007040070040](https://doi.org/10.1007/s007040070040)
- 1351
- 1352 Mears CA, Wentz FJ, Thorne PW, Bernie D (2011) Assessing uncertainty in estimates of atmospheric temperature changes from MSU and AMSU using a Monte-Carlo estimation technique. *J Geophys Res Atmos* 116:2156–2202
- 1353
- 1354 Nicolis C (1993) Optimizing the global observational network—a dynamical-approach. *J Appl Meteor* 32:1751–1759
- 1355
- 1356 Parker DE (2006) A demonstration that large-scale warming is not urban. *J Clim* 19:2882–2895 doi:[10.1175/JCLI3730.1](https://doi.org/10.1175/JCLI3730.1)
- 1357
- 1358 Peterson TC (2003) Assessment of urban versus rural in situ surface temperatures in the contiguous United States: No difference found. *J Clim* 16:2941–2959
- 1359
- 1360 Pielke RA et al (2007) Unresolved issues with the assessment of multidecadal global land surface temperature trends. *J Geophys Res (Atmos)*. 112, 2156–2202. doi:[10.1029/2006JD008229](https://doi.org/10.1029/2006JD008229)
- 1361
- 1362 Pinel J, Lovejoy S, Schertzer D (2014) The horizontal space-time scaling and cascade structure of the atmosphere and satellite radiances. *Atmos Resear* 140–141:95–114 doi:[10.1016/j.atmosres.2013.11.022](https://doi.org/10.1016/j.atmosres.2013.11.022)
- 1363
- 1364 Rohde R, Muller RA, Jacobsen R, Muller E, Perlmutter S, Rosenfeld A, Wurtele J, Groom D, Wickham C (2013) A New Estimate of the Average Earth Surface Land Temperature Spanning 1753 to 2011. *Geoinfor Geostat: An Overview*. doi:[10.4172/2327-4581.1000101](https://doi.org/10.4172/2327-4581.1000101)
- 1365
- 1366 Rybski D, Bunde A, Havlin S, von Storch H (2006) Long-term persistence in climate and the detection problem. *Geophys Resear Lett* 33:L06718-06711-06714 doi:[10.1029/2005GL025591](https://doi.org/10.1029/2005GL025591)
- 1367
- 1368 Rypdal K, Østvand L, Rypdal M (2013) Long-range memory in Earth’s surface temperature on time scales from months to centuries. *JGR Atmos* 118:7046–7062 doi:[10.1002/jgrd.50399](https://doi.org/10.1002/jgrd.50399)
- 1369
- 1370 Smith TM, Reynolds RW, Peterson TC, Lawrimore J (2008) Improvements to NOAA’s Historical Merged Land-Ocean Surface Temperature Analysis (1880–2006). *J Clim* 21:2283–2293
- 1371
- 1372 Veneziano D, Langousis A (2005) The areal reduction factor: a multifractal analysis. *Water Resour Res*. doi:[10.1029/2004WR003765](https://doi.org/10.1029/2004WR003765)
- 1373
- 1374 Williams CN, Menne M, Lawrimore JH (2012) NCDC Technical Report No. GHCNM-12-02 Modifications to Pairwise Homogeneity Adjustment software to address coding errors and improve run-time efficiency Rep., NOAA, Washington DC
- 1375
- 1376
- 1377
- 1378
- 1379
- 1380
- 1381
- 1382
- 1383
- 1384
- 1385
- 1386
- 1387
- 1388
- 1389
- 1390
- 1391
- 1392
- 1393
- 1394
- 1395
- 1396
- 1397
- 1398
- 1399
- 1400
- 1401
- 1402
- 1403
- 1404
- 1405
- 1406
- 1407
- 1408
- 1409
- 1410
- 1411
- 1412
- 1413
- 1414
- 1415
- 1416
- 1417
- 1418
- 1419